# ADAPTIVITY AND A POSTERIORI ERROR CONTROL FOR BIFURCATION PROBLEMS III: INCOMPRESSIBLE FLUID FLOW IN OPEN SYSTEMS WITH $O(2)$ SYMMETRY

K. ANDREW CLIFFE *, EDWARD J.C. HALL †, PAUL HOUSTON ‡, ERIC T. PHIPPS §, AND ANDREW G. SALINGER ¶

**Abstract.** In this article we consider the *a posteriori* error estimation and adaptive mesh refinement of discontinuous Galerkin finite element approximations of the bifurcation problem associated with the steady incompressible Navier–Stokes equations. Particular attention is given to the reliable error estimation of the critical Reynolds number at which a steady pitchfork bifurcation occurs when the underlying physical system possesses rotational and reflectional or $O(2)$ symmetry. Here, computable *a posteriori* error bounds are derived based on employing the generalization of the standard Dual Weighted Residual approach, originally developed for the estimation of target functionals of the solution, to bifurcation problems. Numerical experiments highlighting the practical performance of the proposed *a posteriori* error indicator on adaptively refined computational meshes are presented. Here, particular attention is devoted to the problem of flow through a cylindrical pipe with a sudden expansion, which represents a notoriously difficult computational problem.

**Key words.** Incompressible flows, bifurcation problems, *a posteriori* error estimation, adaptivity, discontinuous Galerkin methods, $O(2)$ symmetry

## 1. Introduction.

In this article, we study the stability of the three–dimensional incompressible Navier-Stokes equations in the case when the underlying system possesses both rotational and reflectional symmetry, or more precisely, $O(2)$ symmetry. To this end, we are interested in numerically estimating the critical Reynolds number $Re$, at which a (pitchfork) bifurcation point first occurs; a review of techniques for bifurcation detection can be found in Cliffe *et al.* [13], for example. The work in this article expands upon our recent work in [12] and [10] to include problems whose geometries exhibit both rotational and reflectional symmetry. The detection of bifurcation points in this setting is now well understood, for example, see Golubitsky and Schaeffer [19]. For the purposes of this article, we assume that a symmetric steady state solution to the incompressible Navier-Stokes equations undergoes a steady pitchfork bifurcation at a critical value of the Reynolds number. Estimation of the critical $Re$ can be undertaken by either investigating the nature of eigenvalues arising from the discretization of the underlying linearised PDE at a specific Reynolds number or by discretizing a suitable extended system of partial differential equations; see Brezzi *et al.* [8] and Werner and Spence [28] for steady bifurcations. For discretization purposes we exploit the interior penalty discontinuous Galerkin (DG) method [4, 16, 14], primarily due to the benefits in stability and mesh adaptivity it affords us. The derivation of a computable error estimator for the critical parameter of interest, namely $Re$, based on exploiting the Dual Weighted Residual (DWR) *a posteriori* error

* School of Mathematical Sciences, University of Nottingham, University Park, Nottingham NG7 2RD, UK, email: Andrew.Cliffe@nottingham.ac.uk.

† School of Mathematical Sciences, University of Nottingham, University Park, Nottingham NG7 2RD, UK, email: Edward.Hall@nottingham.ac.uk. The research of this author was supported by the EPSRC under grant EP/E013724/1.

‡ School of Mathematical Sciences, University of Nottingham, University Park, Nottingham NG7 2RD, UK, email: Paul.Houston@nottingham.ac.uk.

§Computer Science Research Institute, Sandia National Laboratories, Albuquerque, New Mexico, email: etphipp@sandia.gov.

¶Computer Science Research Institute, Sandia National Laboratories, Albuquerque, New Mexico, email: agsalin@sandia.gov.

estimation technique is undertaken and implemented within an adaptive finite element algorithm. The application of this approach to study steady pitchfork bifurcations highlights the numerical performance of the error estimation techniques developed in this article. To the best of our knowledge, our article represents the first attempt to derive *a posteriori* error bounds on critical parameter values for the hydrodynamic stability problem in the $O(2)$ setting.

The flow of a viscous fluid through a channel with a sudden expansion has been well understood for two decades since the physical and computational work carried out by Fearn *et al.* [18], both of which confirmed the presence of a symmetry breaking bifurcation at a Reynolds number of $Re \approx 40$, cf. also [10]. In contrast, flow through a cylindrical pipe with a sudden expansion remains poorly understood. Recent experimental results by Mullin *et al.* [25] have gone some way to increase understanding of the behaviour of the flow in this setting, indicating the loss of stability of a symmetric solution at a Reynolds number of $Re \approx 1200$. The techniques developed in this article for the accurate location of steady bifurcation points will be applied to this problem of flow in a suddenly expanding pipe and the results compared with the experimental data presented in [25].

The paper is structured as follows. In the next section we discuss the general approach adopted for detecting the location at which a bifurcation may occur from a steady state solution of an abstract time dependent problem; we then show how we can utilize $O(2)$ symmetry in the underlying geometry of the problem to reduce computational complexity. Assuming a finite element type discretization of the underlying bifurcation problem, we then proceed in Section 4 to describe how the DWR *a posteriori* error estimation technique can be utilized to approximate the error between the true critical parameter and the computed one. A detailed discussion concerning the reduction of the computational complexity of the discretized bifurcation problem and the associated dual problem then follows in Section 5. We then turn our attention to the specific problem of hydrodynamic stability: this includes the formulation of the DG discretization of the incompressible Navier-Stokes equations in cylindrical coordinates and their appropriate linearization. In Section 7 we investigate the practical performance of the proposed *a posteriori* error estimator on sequences of adaptively generated meshes for two well-documented test cases. In particular, the quality of the (approximate) error representation and (approximate) *a posteriori* bound are studied through these numerical examples. We then apply the techniques developed in this article alongside those developed in [11] to the problem of a sudden expansion in a cylindrical pipe. Finally, we summarize the work presented in this article and draw some conclusions in Section 8.

**2. Detecting steady bifurcation points.** Suppose we have a nonlinear, time dependent problem of the form

$$\frac{\partial u}{\partial t} + F(u, \lambda) = 0, \tag{2.1}$$

where $F$ is a map from $V \times \mathbb{R} \to V$, for some Banach space $V$, with norm $\|\cdot\|$. Here, $\lambda$ is some distinguished parameter, *e.g.* a flow rate or Reynolds number, and $u$ is a state variable, *e.g.* a temperature or velocity field. Our goal is to investigate the linear stability of steady state solutions of (2.1) and to locate the critical parameter value at which solutions lose stability and bifurcations occur. Before we proceed we make the assumption that $F$ is smooth, that is, $F$ is a $C^p$ mapping for $p \geq 3$. We denote the Fréchet derivative of $F$ with respect to $u$ at a fixed point $(w, \chi) \in V \times \mathbb{R}$ by $F'_u(w, \chi; \cdot)$

and similarly the derivative with respect to $\lambda$ by $F'_\lambda(w,\chi)$. Here and throughout this article, we use the convention that in semi-linear forms such as $F'_u(\cdot,\cdot;\cdot)$ the form is linear with respect to all arguments to the right of the semicolon. We will assume that $F'_u(u,\lambda;\cdot) : V \to V$ is Fredholm of index 0 for all $(u,\lambda) \in V \times \mathbb{R}$. For convenience, at a given point $(u^0,\lambda^0)$, we define

$$F^0 := F(u^0,\lambda^0),\ F^0_u(\cdot) := F'(u^0,\lambda^0;\cdot) \text{ and } F^0_\lambda := F'_\lambda(u^0,\lambda^0).$$

Higher order Fréchet derivatives are expressed in much the same way, for example, the Fréchet derivative of $F'_u(w,\chi,\cdot)$ with respect to $u$ at a fixed point $v$ is denoted by $F''_{uu}(w,\chi;\cdot,v)$ and similarly, at a given point $(u^0,\phi^0,\lambda^0)$, we define

$$F^0_{uu}\phi^0(\cdot) := F''_{uu}(u^0,\lambda^0;\cdot,\phi^0) \text{ and } F^0_{u\lambda}\phi^0 := F''_{u\lambda}(u^0,\lambda^0;\phi^0).$$

We investigate the linear stability of steady state solutions $u^0$ at specific parameter values $\lambda^0$, found by solving the steady version of (2.1), *i.e.*,

$$F^0 = 0. \tag{2.2}$$

To consider the growth of small perturbations away from $u^0$, we assume that the solution is of the form $u = u^0 + \phi e^{-\mu t}$. Thereby, after linearization, from (2.1) we deduce the eigenvalue problem:

$$F^0_u(\phi) = \mu\phi. \tag{2.3}$$

The nature of the eigenvalues of (2.3) determine the stability of the steady state solution $u^0$. A change in sign of the real part of any of the eigenvalues from positive to negative indicates a loss of stability. We shall refer to the eigenvalues with smallest real part as the *most dangerous* ones and investigate when these most dangerous eigenvalues first cross the imaginary axis. If a single real–valued eigenvalue crosses the imaginary axis, then a steady bifurcation occurs; on the other hand, if a complex conjugate pair cross the imaginary axis then a Hopf bifurcation occurs, in which case a time dependent solution will exist. Throughout this paper we will be concerned only with steady bifurcations, however, for the application of the methodology employed in this article to Hopf bifurcations, see [11, 10], where problems exhibiting $Z_2$–symmetry are considered. In [11] we considered the application of the DWR *a posteriori* error estimation technique to compute the eigenvalues $\mu$ for a series of parameter values $\lambda^0$, while in [10] the error estimation was directed specifically at computing the *critical parameter value*, *i.e.* the value where the steady solution first loses stability.

Hence, we can either test various parameter values $\lambda^0$ and investigate the nature of the eigenvalues arising, in which case we are effectively computing $\mathbf{u}^0 = (u^0,\phi^0,\mu^0)$ which solves the system of equations

$$E(\mathbf{u}^0) \equiv \begin{pmatrix} F^0 \\ F^0_u(\phi^0) - \mu^0\phi^0 \end{pmatrix} = \mathbf{0}, \tag{2.4}$$

or, alternatively, we can seek to find directly the critical parameter value which has an eigenvalue with zero real part. To this end, for a steady bifurcation we recast equations (2.2)–(2.3) in the following extended system form, where we have dropped the superscript "0" for notational simplicity: find $\mathbf{u} := (u,\phi,\lambda)$ such that

$$T(\mathbf{u}) \equiv \begin{pmatrix} F(u,\lambda) \\ F'_u(u,\lambda;\phi) \\ \langle\phi, g\rangle - 1 \end{pmatrix} = \mathbf{0}, \tag{2.5}$$

where $\langle \cdot, \cdot \rangle$ denotes the duality pairing between the spaces $V$ and $V'$, $V'$ being the dual space of $V$, and $g \in V'$ is some suitable functional satisfying $\langle \phi, g \rangle \neq 0$. The equation $\langle \phi, g \rangle - 1 = 0$ acts to normalise the nullfunction $\phi$, thus ensuring that, if a solution to (2.5) exists at some $\lambda$, the solution is unique.

Before we begin the discussion of how to detect steady bifurcations in the presence of $O(2)$ symmetry, we state the following lemma, which will prove useful.

LEMMA 2.1 ('ABCD' Lemma). *Let $V$ be a Banach Space and consider the linear operator $M : V \times \mathbb{R} \to V \times \mathbb{R}$ of the form*

$$M := \begin{pmatrix} A & b \\ \langle \cdot, c \rangle & d \end{pmatrix}, \tag{2.6}$$

*where $A : V \to V$, $b \in V \backslash \{0\}$, $c \in V \backslash \{0\}$, $d \in \mathbb{R}$. Then*

1. *If $A$ is an isomorphism on $V$, then $M$ is an isomorphism on $V \times \mathbb{R}$ iff $d - (A^{-1}b, c) \neq 0$.*
2. *If $\dim \ker(A) = \operatorname{codim} \operatorname{Range}(A) = 1$, then $M$ is an isomorphism iff*
   *(a) $\langle b, \psi \rangle \neq 0 \quad \forall \psi \in \ker(A^*) \backslash \{0\}$,*
   *(b) $\langle \phi, c \rangle \neq 0 \quad \forall \phi \in \ker(A) \backslash \{0\}$.*
3. *If $\dim \ker(A) \geq 2$, then $M$ is singular.*

*Proof.* See Keller [22]. □

**3. Bifurcation in the presence of $O(2)$ symmetry.** We now discuss how to reduce the complexity of (2.4) and (2.5) when the problem at hand possesses some underlying symmetry, in our case $O(2)$ symmetry. The importance of symmetry in bifurcation problems is well known and many of the key concepts, including the connection with group representation theory, may be found in the books by Vanderbauwhede [27], Golubitsky and Schaeffer [19], and Golubitsky *et al.* [20]. The essential idea is that under the action of a group and for an appropriately chosen basis, the Jacobian of a nonlinear problem 'block-diagonalizes', which in turn leads to significant computational savings. With this in mind, we recall that $O(2)$ is the Lie group which comprises rotations and reflections. More formally $O(2)$ is generated by rotations $r_\alpha$, $\alpha \in \mathbb{R}$, and a reflection $s$, satisfying for any $\alpha$, $\beta \in \mathbb{R}$,

$$r_{\alpha+2\pi} = r_\alpha, \quad r_{\alpha+\beta} = r_\alpha r_\beta = r_\beta r_\alpha, \quad s^2 = r_0 = r_{2\pi} = I, \quad s r_\alpha = r_{-\alpha} s, \tag{3.1}$$

where $I$ is the group identity. $O(2)$ acts (linearly) on $V$ if there exists a continuous mapping $O(2) \times V \to V$ given by $(\gamma, u) \mapsto \gamma u$, which satisfies the following properties.

a) For every $\gamma \in O(2)$ the mapping $\rho_\gamma : V \to V$, defined by $\rho_\gamma u := \gamma u$, is linear.
b) If $\gamma_1, \gamma_2 \in O(2)$ then $(\gamma_1 \gamma_2) u = \gamma_1 (\gamma_2 u)$.

Furthermore, the mapping $\rho$ that relates $\gamma \in O(2)$ to $\rho_\gamma$ is called the representation of $O(2)$ on $V$.

In this section we again consider the steady variant of the nonlinear problem (2.1): find $u$ such that

$$F(u, \lambda) = 0,$$

where additionally we assume that $F$ is $O(2)$ equivariant; cf. below.

DEFINITION 3.1 (Equivariance). *A nonlinear operator $F(\cdot) : V \to V$ is $O(2)$ equivariant if $\forall \gamma \in O(2)$ and $u \in V$*

$$\rho_\gamma F(u) = F(\rho_\gamma u). \tag{3.2}$$

REMARK 3.2. *Equivariance implies that, if $u$ solves $F(u) = 0$, then for any $\gamma \in O(2)$, $\rho_\gamma u$ is also a solution.*

We introduce the notion of $O(2)$ invariant spaces, through the following definition.

DEFINITION 3.3. *A subspace $V^m \subset V$ is $O(2)$ invariant if for all $\gamma \in O(2)$*

$$\rho_\gamma : V^m \to V^m.$$

We are specifically interested in bifurcations away from paths of steady $O(2)$ symmetric solutions and, with this is mind, define the symmetric subspace $V^{O(2)}$ of $V$ by

$$V^{O(2)} := \{v \in V : \rho_\gamma v = v\},$$

for $\gamma \in O(2)$. We notice immediately that, as a consequence of (3.2), $V^{O(2)}$ is invariant under $F$, if $F$ is $O(2)$ equivariant. Thus, upon defining $F^{O(2)}$ as the restriction of $F$ to $V^{O(2)}$, steady $O(2)$ symmetric solutions of (2.1) may be computed by solving the reduced problem

$$F^{O(2)}(u, \lambda) = 0, \quad u \in V^{O(2)}. \tag{3.3}$$

Moreover, taking the Fréchet derivative of (3.2) with respect to $u$ gives

$$\rho_\gamma F'_u(u, \lambda; \phi) = F'_u(\rho_\gamma u, \lambda; \rho_\gamma \phi) \quad \forall \phi \in V.$$

In particular, if $u \in V^{O(2)}$, then we have

$$\rho_\gamma F'_u(u, \lambda; \phi) = F'_u(u, \lambda; \rho_\gamma \phi) \quad \forall \phi \in V.$$

Thereby, in the case when $u \in V^{O(2)}$, the linearized operator $F'_u(u, \lambda; \cdot)$ is also $O(2)$ equivariant.

It is a standard result, see Aston [5], that, for the $O(2)$ case, there exists a unique orthogonal decomposition of $V$, namely,

$$V = \sum_{m=0}^{\infty} V^m, \quad V^m \perp V^l, \quad m \neq l, \tag{3.4}$$

where each $V^m$ is an $O(2)$ invariant subspace of $V$, with the property that $V^m$ is irreducible, *i.e.*, $V^m$ has no proper $O(2)$ invariant subspaces. In fact, as one may expect, the $V^m$ are spanned by the $m$th order Fourier modes of $V$ and $V^0 = V^{O(2)}$.

The key observation essential for reducing the complexity of the underlying bifurcation problem is the following: given an $O(2)$ equivariant operator $A : V \to V$, then $V^m$ are invariant under the action of $A$. That is,

$$A : V^m \to V^m, \quad m = 0, 1, 2, \ldots, \tag{3.5}$$

see Aston [5]. Thereby, for $u \in V^{O(2)}$, our Jacobian operator $F'_u(u, \lambda; \cdot)$ has a diagonal block structure; more precisely the following result holds.

LEMMA 3.4. *Suppose $u \in V^{O(2)}$, then $\mu$ is an eigenvalue of*

$$F'_u(u, \lambda; \phi) = \mu\phi, \quad \phi \in V,$$

*if and only if $\mu$ is also an eigenvalue of*

$$F'_u(u,\lambda;\phi) = \mu\phi, \quad \phi \in V^m. \tag{3.6}$$

*Proof.* See Cliffe *et al.* [13]. □

The decomposition (3.4) is produced purely by the rotation elements $r_\alpha$ of $O(2)$ and the fact that there is also a reflection element has not been used. Indeed, there is a finer decomposition

$$V^m = V^{m,s} \oplus V^{m,a}, \quad m = 1, 2, \ldots,$$

where $V^{m,s}$ and $V^{m,a}$ are the symmetric and anti–symmetric components of $V^m$, respectively. Further, $V^{m,s}$ and $V^{m,a}$ are invariant subspaces of $V$ with respect to the reflection $s$, hence, equation (3.6) can be further reduced to

$$\mu \begin{pmatrix} \phi^s \\ \phi^a \end{pmatrix} = \begin{pmatrix} F'_u(u,\lambda;\phi^s) \\ F'_u(u,\lambda;\phi^a) \end{pmatrix}, \quad m = 1, 2, \ldots, \tag{3.7}$$

where $\phi^s \in V^{m,s}$ and $\phi^a \in V^{m,a}$. Crucially, $F'_u(u,\lambda;\cdot)|_{V^{m,s}} = F'_u(u,\lambda;\cdot)|_{V^{m,a}}$, thus, for $m = 1, 2, \ldots$, any eigenvalue of $F'_u(u,\lambda;\cdot)|_{V^m}$ has a geometric multiplicity of 2; see Aston [5] for further details.

Hence, for a specific parameter value $\lambda^0$ we can determine the eigenvalues of symmetric steady state solutions by solving, for $m = 0, 1, 2, \ldots$, the reduced problem: find $\mathbf{u}^0 = (u^0, \phi^0, \mu^0) \in V^{O(2)} \times V^{m,s} \times \mathbb{R}$ (or equivalently $\mathbf{u}^0 = (u^0, \phi^0, \lambda^0) \in V^{O(2)} \times V^{m,a} \times \mathbb{R}$) such that

$$E(\mathbf{u}^0) \equiv \begin{pmatrix} F^0 \\ F^0_u(\phi^0) - \mu^0\phi^0 \end{pmatrix} = \mathbf{0}; \tag{3.8}$$

here, for $m = 0$, $\phi^0$ is sought in $V^0 = V^{O(2)}$. In an identical manner, we can locate critical parameter values at which symmetric steady state solutions $u \in V^{O(2)}$ lose stability by solving the following problems for $m = 0, 1, \ldots$: find $\mathbf{u} = (u, \phi, \lambda) \in V^{O(2)} \times V^{m,s} \times \mathbb{R}$ (or equivalently $\mathbf{u} = (u, \phi, \lambda) \in V^{O(2)} \times V^{m,a} \times \mathbb{R}$) such that

$$T(\mathbf{u}) \equiv \begin{pmatrix} F(u,\lambda) \\ F'_u(u,\lambda;\phi) \\ \langle \phi, g \rangle - 1 \end{pmatrix} = \mathbf{0}, \tag{3.9}$$

where $g \in V'$ is some suitable functional satisfying $\langle \phi, g \rangle \neq 0$, and, as above, for $m = 0$, $\phi$ is sought in $V^0 = V^{O(2)}$. The result is that the original problem can be divided up into a series of problems with reduced complexity. Throughout the rest of this article we shall assume the physically more interesting case where the steady state solutions first become unstable with $m \neq 0$, in which case there is a symmetry breaking bifurcation, rather than just a turning point or fold point. In addition, we assume that we have a bifurcation of pitchfork type, for which the constraints are gathered in the following theorem.

THEOREM 3.5. *Let $u(\lambda_0) \in V^{O(2)}$. Suppose that*

$$\text{Null}(F^0_u(\cdot)) \subset V^m, \quad m \neq 0,$$

*$\mu = 0$ is a simple eigenvalue,* i.e.

$$\dim(\text{Null}(F^0_u(\cdot) \cap V^s) = 1 \quad \textit{and} \quad \dim(\text{Null}(F^0_u(\cdot) \cap V^a) = 1,$$

*where* $V^s = \{u : su = u\}$ *and* $V^a = \{u : su = -u\}$*, the symmetric and anti-symmetric elements of* $V$*. Finally, let*

$$b_\lambda := \langle F'_{u\lambda}(u, \lambda; \phi) + F''_{uu}(u, \lambda; w, \phi), \psi\rangle \neq 0, \tag{3.10}$$

*where* $\psi \in \ker((F_u^*)$ *for* $F_u^*$ *the adjoint of* $F'_u(u, \lambda, \cdot)$ *and* $w \in V^s$ *solves* $F'_u(u, \lambda; w) + F'_\lambda(u, \lambda) = 0$*.*

*Then there exists a secondary branch of* $O(2)$ *symmetry breaking solutions. The bifurcation is of pitchfork type and the bifurcating branch has* $D_m$ *symmetry. Here,* $D_m$ *is the dihedral group generated by* $r_{2\pi/m}$ *and* $s$*.*

We would also like to determine sub- or supercriticality of a bifurcation point. To this end we must calculate a term involving third order derivatives of $F$:

$$d := \langle \psi, F'''_{uuu}(u, \lambda, \phi, \phi, \phi) + 3F''_{uu}(u, \lambda, \phi, z)\rangle \tag{3.11}$$

where $\psi \in \mathrm{Null}(F_u^*(\cdot)) \cap V^s$ and $z \in H^{O(2)} \oplus V^{2m}$ is the unique solution of

$$F'_u(u, \lambda, z) + F''_{uu}(u, \lambda, \phi, \phi) = 0.$$

Then, the following lemma holds.

LEMMA 3.6. *Let* $b_\lambda$ *and* $d$ *be defined as in (3.10) and (3.11) respectively. Then, assuming* $d/b_\lambda \neq 0$*, the bifurcation is supercritical if* $d/b_\lambda < 0$ *and subcritical if* $d/b_\lambda > 0$*.*

*Proof.* See [13]. □

**4. *A posteriori* error estimation.** In this section we develop a general theoretical framework for the derivation of computable *a posteriori* error estimates for the error in the computed bifurcation point when the extended system (3.9) is numerically approximated by a general Galerkin finite element method. To this end, we exploit the duality-based *a posteriori* error estimation techniques developed by C. Johnson and R. Rannacher and their collaborators. For a detailed discussion, we refer to the series of articles [6, 21, 17, 23]. We remark that, in the discussion that follows, we concentrate only on error estimation for the critical parameter value found using (3.9); error estimation of the eigenvalue can be performed in an analogous manner, see Cliffe *et al.* [11].

We begin by first introducing a suitable finite element approximation of the bifurcation problem (3.9). To this end, we consider a sequence of $O(2)$ symmetric finite element spaces $V_{h,p}^0$ and finite elements spaces $V_{h,p}^m$ consisting of piecewise polynomial functions of degree $p$ on a partition $\mathcal{T}_h$ of granularity $h$, from which we shall approximate the $O(2)$ symmetric steady solution and the $m$th (symmetric or antisymmetric) nullfunction, respectively.

We find the triple $\mathbf{u}_h = (u_h, \phi_h, \lambda_h) \in \mathbf{V}_{h,p} := V_{h,p}^0 \times V_{h,p}^m \times \mathbb{R}$, $m = 1, 2, \ldots$ such that

$$\begin{aligned}\mathcal{N}(\mathbf{u}_h; \mathbf{v}_h) = \hat{\mathcal{N}}(u_h, \lambda_h; \phi_h, v_h) + \hat{\mathcal{N}}'_u(u_h, \lambda_h; \phi_h, \varphi_h)\\ + \chi_h((g, \phi_h) - 1) = 0 \quad \forall \mathbf{v}_h \in \mathbf{V}_{h,p},\end{aligned} \tag{4.1}$$

where $\mathbf{v}_h := (v_h, \varphi_h, \chi_h)$, $(\cdot, \cdot)$ denotes the standard $L^2$-inner product, $\hat{\mathcal{N}}(\cdot; \cdot)$ is the semi-linear form associated with the discretization of the underlying steady state partial differential equation (2.2) and $\hat{\mathcal{N}}'_u(\cdot, \cdot; \cdot, \cdot)$ is the Jacobian of $\hat{\mathcal{N}}(\cdot; \cdot)$ with respect

to $u$ and thus represents the discretization of $F'_u(\cdot,\cdot;\cdot)$. Further, we shall assume that $(u_h, \phi_h, \lambda_h)$ also satisfies the discrete analogue of the conditions of a pitchfork bifurcation (3.10), that is,

$$\hat{\mathcal{N}}''_{u\lambda}(u_h, \lambda_h; \phi_h, \psi_h) + \hat{\mathcal{N}}''_{uu}(u_h, \lambda_h; w_h, \phi_h, \psi_h) \neq 0, \tag{4.2}$$

where $\psi_h \in \ker(\hat{N}'_u(u_h, \lambda_h; v_h, \cdot))\ \forall v_h$ and $w_h \in V^0_{h,p}$ is the solution to

$$\hat{\mathcal{N}}'_u(u_h, \lambda_h; w_h, \varphi_h) + \hat{\mathcal{N}}'_\lambda(u_h, \lambda_h; \varphi_h) = 0, \quad \forall \varphi_h \in V^m_{h,p}.$$

REMARK 4.1. *We remark that, in a slight variation to the standard approach of the location of critical parameters, we have recast the equations* $(g, \phi_h) - 1 = 0$ *and* $(g, \psi_h) = 0$ *in the weak form* $\chi_h((g, \phi_h) - 1) = 0$ *for all* $\chi_h \in \mathbb{R}$. *As* $\mathbb{R} = \text{span}\{1\}$ *this has no effect when calculating the approximate critical parameter, but this formulation is required for the error estimation which follows.*

For the proceeding error analysis we make the assumption that (4.1) is consistent, that is, for the analytical solution $\mathbf{u}$ of (3.9) satisfies

$$\mathcal{N}(\mathbf{u}, \mathbf{v}_h) = 0 \quad \forall \mathbf{v}_h \in \mathbf{V}_{h,p}. \tag{4.3}$$

**4.1. DWR approach for functionals.** For a linear target functional of practical interest $J(\cdot)$, we briefly outline the key steps involved in estimating the approximation error $J(\mathbf{u}) - J(\mathbf{u}_h)$ employing the DWR technique. We write $\mathcal{M}(\cdot,\cdot;\cdot,\cdot)$ to denote the mean value linearization of $\mathcal{N}(\cdot;\cdot)$, defined by

$$\begin{aligned}\mathcal{M}(\mathbf{u}, \mathbf{u}_h; \mathbf{u} - \mathbf{u}_h, \mathbf{w}) &= \mathcal{N}(\mathbf{u}; \mathbf{w}) - \mathcal{N}(\mathbf{u}_h; \mathbf{w}) \\ &= \int_0^1 \mathcal{N}'_{\mathbf{u}}(\theta\mathbf{u} + (1-\theta)\mathbf{u}_h; \mathbf{u} - \mathbf{u}_h, \mathbf{w})\, \mathrm{d}\theta,\end{aligned} \tag{4.4}$$

for some $\mathbf{w} \in \hat{\mathbf{V}}$. Here, $\hat{\mathbf{V}}$ is some suitably chosen space such that $\mathbf{V}_{h,p} \subset \hat{\mathbf{V}}$. We now introduce the following (formal) *dual problem*: find $\mathbf{z} \in \hat{\mathbf{V}}$ such that

$$\mathcal{M}(\mathbf{u}, \mathbf{u}_h; \mathbf{w}, \mathbf{z}) = J(\mathbf{w}) \quad \forall \mathbf{w} \in \hat{\mathbf{V}}. \tag{4.5}$$

We assume that (4.5) possesses a unique solution. This assumption is, of course, dependent on both the definition of $\mathcal{M}(\mathbf{u}, \mathbf{u}_h; \cdot, \cdot)$ and the target functional under consideration. For the proceeding error analysis, we must therefore assume that (4.5) is well–posed. By using the linearity of $J(\cdot)$, combining (4.4), and (4.5) and using the consistency condition (4.3) we arrive at the following error representation formula

$$\begin{aligned}J(\mathbf{u}) - J(\mathbf{u}_h) = J(\mathbf{u} - \mathbf{u}_h) &= \mathcal{M}(\mathbf{u}, \mathbf{u}_h; \mathbf{u} - \mathbf{u}_h, \mathbf{z}) \\ &= \mathcal{M}(\mathbf{u}, \mathbf{u}_h; \mathbf{u} - \mathbf{u}_h, \mathbf{z} - \bar{\mathbf{z}}_h) \\ &= -\mathcal{N}(\mathbf{u}_h, \mathbf{z} - \bar{\mathbf{z}}_h) \quad \forall \bar{\mathbf{z}}_h \in \mathbf{V}_{h,p}.\end{aligned} \tag{4.6}$$

In practice (4.6) must be numerically estimated by computing a suitable approximation $\mathbf{z}_h$ to the dual solution $\mathbf{z}$. Note that any $\mathbf{z}_h \in \mathbf{V}_{h,p}$ results in the error representation formula being identically equal to zero, due to (4.1). Thereby, a number of possible alternatives exist: the first involves keeping the degree $p$ of the approximating polynomial the same as that for $\mathbf{u}_h$, but computing $\mathbf{z}_h$ on a sequence of dual finite element meshes $\hat{\mathcal{T}}_{\hat{h}}$ which, in general, differ from the "primal meshes" $\mathcal{T}_h$. Alternatively, $\mathbf{z}_h \in \mathbf{V}_{h,\hat{p}}$ may be computed using polynomials of degree $\hat{p} > p$ on the same

finite element mesh $\mathcal{T}_h$ employed for the primal problem. A variant of this second approach is to compute the approximate dual solution using the same polynomial degree $p$ as used for the primal problem and to extrapolate the resulting approximate dual solution $\mathbf{z}_h$. Although this latter approach is the cheapest of the three methods, and is still capable of producing adaptively refined meshes specifically tailored to the selected target functional, the quality of the resulting approximate error representation formula may be poor. On the basis of numerical experimentation, we favour the second approach due to its computational simplicity of implementation.

In our case we are interested in controlling the error in the critical bifurcation parameter and hence the target functional of interest is simply $J(\mathbf{u}) = \lambda$. As the dual problem involves the true solution $\mathbf{u}$ we must commit a linearization error and use the approximate $\mathbf{u}_h$ instead. Thereby, the dual problem we actually solve for estimating the error in the approximate critical parameter is given by: find $\mathbf{z}_h := (z_u; z_\phi, z_\lambda) \in \mathbf{V}_{h,\hat{p}}$ such that

$$\begin{aligned} \hat{\mathcal{N}}'_u(u_h, \lambda_h; v_h, z_u) + \hat{\mathcal{N}}'_\lambda(u_h, \lambda_h; z_u)\chi_h \\ + \hat{\mathcal{N}}''_{uu}(u_h, \lambda_h; \varphi_h, \phi_h, z_\phi) + \hat{\mathcal{N}}'_u(u_h, \lambda_h; \varphi_h, z_\phi) \\ + \hat{\mathcal{N}}''_{u\lambda}(u_h, \lambda_h; \phi_h, z_\phi)\chi_h + z_\lambda(g, \varphi_h) = 1 \quad \forall \mathbf{v}_h \in \mathbf{V}_{h,\hat{p}}, \end{aligned} \tag{4.7}$$

where $\mathbf{v}_h := (v_h, \varphi_h, \chi_h)$.

**5. Solution procedure.** In this section we discuss how to solve the primal and dual problems arising in the previous section in an efficient manner by reducing the extended problems to a succession of smaller ones.

To determine the numerical solution $\mathbf{u}_h$ to the nonlinear system of equations (4.1), we employ a damped Newton method. This nonlinear iteration generates a sequence of approximations $\mathbf{u}_h^n$, $n = 1, 2, \ldots$, to the actual numerical solution $\mathbf{u}_h$ using the following algorithm. Given an iterate $\mathbf{u}_h^n$, the update $\mathbf{d}_h^n := (du_h^n, d\phi_h^n, d\lambda_h^n, )$ of $\mathbf{u}_h^n$ to get to the next iterate

$$\mathbf{u}_h^{n+1} = \mathbf{u}_h^n + \omega^n \mathbf{d}_h^n$$

is defined by: find $\mathbf{d}_h^n$ such that for all $\mathbf{v}_h = (v_h, \varphi_h, \chi_h) \in \mathbf{V}_{h,p}$

$$\begin{aligned} \hat{\mathcal{N}}'_u(u_h^n, \lambda_h^{0,n}; du_h^n, v_h) + \hat{\mathcal{N}}'_\lambda(u_h^n, \lambda_h^n; v_h)d\lambda_h^n &= r_1^n(v_h), \\ \hat{\mathcal{N}}''_{uu}(u_h^n, \lambda_h^n; du_h^n, \phi_h^n, \varphi_h) \\ + \hat{\mathcal{N}}'_u(u_h^n, \lambda_h^n; d\phi_h^n, \varphi_h) + \hat{\mathcal{N}}''_{u\lambda}(u_h^n, \lambda_h^n; \phi_h^n, \varphi_h)d\lambda_h^n &= r_2^n(\varphi_h), \\ \chi_h(d\phi_h^n, c) &= r_3^n(\chi_h). \end{aligned} \tag{5.1}$$

Here, $r_1^n(\cdot)$, $r_2^n(\cdot)$ and $r_3^n(\cdot)$ are residuals given, respectively, by

$$r_1^n(v_h) = -\hat{\mathcal{N}}(u_h^n.\lambda_h^n; v_h),\ r_2^n(\varphi_h) = -\hat{\mathcal{N}}'_u(u_h^n, \lambda_h^n; \phi_h^n, \varphi_h),$$

$$r_3^n(\chi_h) = -\chi_h((\phi_h^n, g) - 1).$$

To reduce the computational complexity, we perform an $LU$-decomposition of the matrices involved in the Newton iterations to reduce the problem to a succession of smaller ones. Assuming a Galerkin type approximation of $\mathbf{u}_h$ is exploited, in which case $u_h^n = \sum_{i=1}^N U_i^n \varphi_i$, $\phi_h^n = \sum_{i=1}^N \Phi_i^n \zeta_i$, where $\{\varphi_i\}_{i=1}^N$ is a basis for $V_{h,p}^0$ and $\{\zeta_i\}_{i=1}^N$

is a basis for $V_{h,p}^{m,s}$. Similarly, we let $du_h^n = \sum_{i=1}^N dU_i^n \varphi_i$ and $d\phi_h^n = \sum_{i=1}^N d\Phi_i^n \zeta_i$. For ease of exposition we define $\boldsymbol{\phi}_h^n = \{\Phi_i^n\}_{i=1}^N$, $\boldsymbol{d}u_h^n = \{dU_i^n\}_{i=1}^N$ and $\boldsymbol{d}\phi_h^n = \{d\Phi_i^n\}_{i=1}^N$ and with an abuse of notation, we may rewrite (5.1) in the following form

$$\begin{bmatrix} F_u^{0,n} & 0 & \boldsymbol{F}_\lambda^{0,n} \\ F_{uu}^{m,n} & F_u^{m,n} & \boldsymbol{F}_{u\lambda}^{m,n} \\ \mathbf{0}^\top & \boldsymbol{l}^\top & 0 \end{bmatrix} \begin{bmatrix} \boldsymbol{d}u_h^n \\ \boldsymbol{d}\phi_h^n \\ d\lambda_h^n \end{bmatrix} = \begin{bmatrix} \boldsymbol{r}_1^n \\ \boldsymbol{r}_2^n \\ r_3^n \end{bmatrix}, \tag{5.2}$$

where the superscript $n$ means evaluation at the $n$th Newton iterate, the superscript 0 indicates evaluation in the space $V_{h,p}^0$ and the superscript $m$ means evaluation in the space $V_{h,p}^{m,s}$, $m = 1, 2, \ldots$. The matrix appearing in (5.2) can then be written in block $LU$ format as:

$$\begin{bmatrix} F_u^{0,n} & 0 & \boldsymbol{F}_\lambda^{0,n} \\ F_{uu}^{m,n} & F_u^{m,n} & \boldsymbol{F}_{u\lambda}^{m,n} \\ \mathbf{0}^\top & \boldsymbol{l}^\top & 0 \end{bmatrix} = LU, \tag{5.3}$$

where

$$L = \left[\begin{array}{c|cc} F_u^{0,n} & 0 & \mathbf{0} \\ \hline F_{uu}^{m,n} & I & \mathbf{0} \\ \mathbf{0}^\top & \mathbf{0}^\top & 1 \end{array}\right] \text{ and } U = \left[\begin{array}{c|cc} I & 0 & -\boldsymbol{w}^{0,n} \\ \hline 0 & F_u^{m,n} & F_{uu}^{m,n}\boldsymbol{w}^{0,n} + \boldsymbol{F}_{u\lambda}^{m,n} \\ \mathbf{0}^\top & \boldsymbol{l}^\top & 0 \end{array}\right],$$

and $\boldsymbol{w}^{0,n}$ satisfies

$$F_u^{0,n}\boldsymbol{w}^{0,n} = -\boldsymbol{F}_\lambda^{0,n}, \tag{5.4}$$

cf. [10]. The foregoing assumptions guarantee that, at the bifurcation point, both $F_u^0$ and the matrix

$$\begin{bmatrix} F_u^{m,n} & F_{uu}^{m,n}\boldsymbol{w}^{0,n} + \boldsymbol{F}_{u\lambda}^{m,n} \\ \boldsymbol{l}^\top & 0 \end{bmatrix} \tag{5.5}$$

evaluated at $(u_h, \lambda_h)$ are nonsingular. Thus, a continuity argument ensures that for $(u_h^n, \phi_h^n, \lambda_h^n)$ sufficiently close to $(u_h, \phi_h, \lambda_h)$ equation (5.2) is soluble. In particular, at each Newton iteration, the solution to the $(2N+1) \times (2N+1)$ matrix problem (5.2) may be computed based on solving two $N \times N$ matrix problems involving $\mathrm{F}_u^{0,n}$, and one $(N+1) \times (N+1)$ matrix problem involving (5.5), together with appropriate forward and backward substitutions. We point out that the first linear solve involving the matrix $\mathrm{F}_u^{0,n}$ is necessary to first compute the vector $\boldsymbol{w}^{0,n}$, cf. (5.4) above, while the second solve is undertaken in the forward substitution employing the matrix $L$. In order that the Newton iteration converges, we must have a good guess for both the steady state solution and the nullfunction. These are achieved using a continuation procedure: the steady solution is first solved for a small parameter and then the most dangerous eigenvalue computed. The parameter is gradually increased until there is a change in sign of the real part of the left most eigenvalue and when this occurs the base solution/eigenfunction pair is used for the initial guess for the Newton iteration.

To solve the approximate dual problem for the steady bifurcation, we first write $z_u = \sum_{i=1}^{\hat{N}} Z_{u,i}\hat{\varphi}_i$, $z_\phi = \sum_{i=1}^{\hat{N}} Z_{\phi,i}\hat{\zeta}_i$, $\boldsymbol{z}_u = \{Z_{u,i}\}_{i=1}^{\hat{N}}$, and $\boldsymbol{z}_\phi = \{Z_{\phi,i}\}_{i=1}^{\hat{N}}$, where $\{\hat{\varphi}_i\}_{i=1}^{\hat{N}}$ and $\{\hat{\zeta}_i\}_{i=1}^{\hat{N}}$ denote a suitable set of linearly independent finite element basis

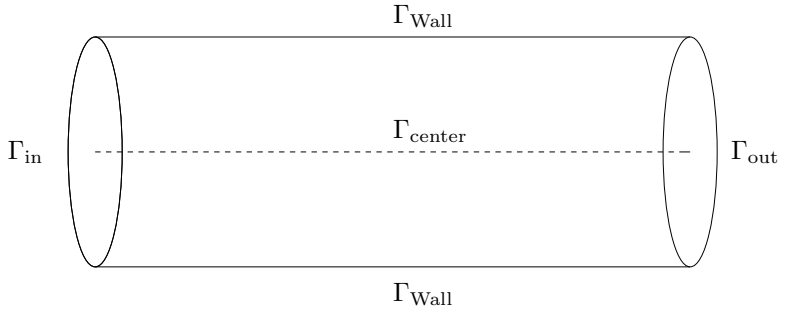


FIG. 6.1. *Generic cylindrical pipe domain.*

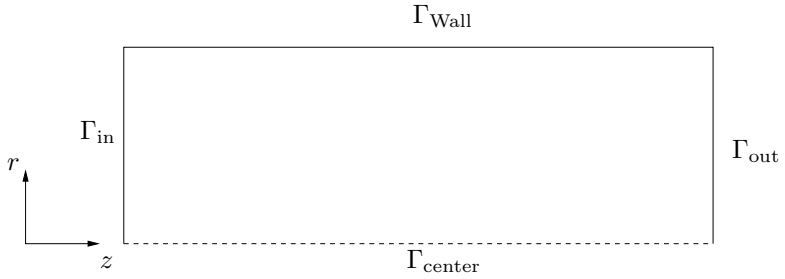


FIG. 6.2. *Radial slice through the pipe domain.*

functions which span $V^0_{h,\hat{p}}$ and $V^{m,s}_{h,\hat{p}}$, respectively. Thus, we can rewrite the dual problem (4.7) as: find the triple $(\boldsymbol{z}_u, \boldsymbol{z}_\phi, z_\lambda)$ satisfying

$$\begin{bmatrix} (\hat{F}^0_u)^\top & (\hat{F}^m_{uu})^\top & \mathbf{0} \\ 0 & (\hat{F}^m_u)^\top & \boldsymbol{l} \\ (\hat{\boldsymbol{F}}^0_\lambda)^\top & (\hat{\boldsymbol{F}}^m_{u\lambda})^\top & 0 \end{bmatrix} \begin{bmatrix} \boldsymbol{z}_u \\ \boldsymbol{z}_\phi \\ z_\lambda \end{bmatrix} = \begin{bmatrix} \mathbf{0} \\ \mathbf{0} \\ 1 \end{bmatrix}. \tag{5.6}$$

Here, $\hat{F}^0_u$ is understood to be the Jacobian on the space $\mathbf{V}_{h,\hat{p}}$ evaluated at $u_h$, and so on. Hence, the matrix involved in the dual solve is no more than the transpose of that used in the Newton solves, albeit on a larger finite dimensional space. Thus, we can use the same LU decomposition proposed above to reduce the complexity of the problem.

**6. Navier–Stokes equations and DG discretization.** In this section we outline the application of the above theory to the problem of incompressible fluid flow in an open system whose geometry has rotational symmetry about a single axis. In particular, for the discretization of the underlying bifurcation problem, we exploit the symmetric version of the interior penalty DG method.

**6.1. Navier–Stokes equations in cylindrical coordinates.** We shall now apply the theory described above to the flow of an incompressible fluid in a generic open cylindrical pipe $\Omega \subset \mathbb{R}^3$, see Figure 6.1, for example. We point out that the proceeding discussion holds for more general computational domains, such as those considered in Section 7. By introducing the Reynolds number $Re$, defined as $Re = Ru_{\max}/\nu$, where $R$ is the radius of the pipe, $u_{\max}$ is the peak inlet velocity and $\nu$ is the kinematic viscosity, the equations governing this flow are the non-dimensionalized incompressible Navier–Stokes equations, which, in cylindrical coordinates and written

in divergence form (to facilitate the DG discretization), are given by

$$\begin{aligned}
\frac{\partial u_z}{\partial t} - \frac{1}{\mathrm{Re}}\nabla^2 u_z + \nabla\cdot(u_z\mathbf{u}) - \frac{1}{2}(\nabla\cdot\boldsymbol{u})u_z + \frac{\partial p}{\partial z} &= 0,\\
\frac{\partial u_r}{\partial t} - \frac{1}{\mathrm{Re}}\left(\nabla^2 u_r - \frac{u_r}{r^2} - \frac{2}{r^2}\frac{\partial u_\phi}{\partial \phi}\right) + \nabla\cdot(u_r\mathbf{u}) - \frac{u_\phi^2}{r} - \frac{1}{2}(\nabla\cdot\boldsymbol{u})u_r + \frac{\partial p}{\partial r} &= 0, \quad (6.1)\\
\frac{\partial u_\phi}{\partial t} - \frac{1}{\mathrm{Re}}\left(\nabla^2 u_\phi - \frac{u_\phi}{r^2} + \frac{2}{r^2}\frac{\partial u_r}{\partial \phi}\right) + \nabla\cdot(u_\phi\mathbf{u}) + \frac{u_r u_\phi}{r} - \frac{1}{2}(\nabla\cdot\boldsymbol{u})u_\phi &\\
+\frac{1}{r}\frac{\partial p}{\partial \phi} &= 0,\\
-\nabla\cdot\mathbf{u} &= 0.
\end{aligned}$$

We note that the term $-\frac{1}{2}(\nabla\cdot\boldsymbol{u})\boldsymbol{u}$ is included to ensure stability of the numerical method, see, for example, [15] and the references cited therein. We shall assume inflow at the boundary $\Gamma_{\mathrm{in}}$, a non-slip condition on $\Gamma_{\mathrm{wall}}$ and natural boundary conditions on $\Gamma_{\mathrm{out}}$. The boundary conditions are therefore

$$\begin{aligned}
&u_z = u_r = u_\phi = 0 \text{ on } \Gamma_{\mathrm{wall}},\\
&u_r = u_\phi = 0, \quad u_z = g_d \text{ on } \Gamma_{\mathrm{in}},
\end{aligned}$$

$$\frac{\partial u_z}{\partial \mathbf{n}} - pn_z = \frac{\partial u_r}{\partial \mathbf{n}} - pn_r = \frac{\partial u_\phi}{\partial \mathbf{n}} - pn_\phi = 0 \text{ on } \Gamma_{\mathrm{out}}.$$

Here,

$$\begin{aligned}
\nabla^2 &:= \frac{\partial^2}{\partial z^2} + \frac{1}{r}\frac{\partial}{\partial r}\left(r\frac{\partial}{\partial r}\right) + \frac{1}{r^2}\frac{\partial^2}{\partial \phi^2},\\
\nabla\cdot\mathbf{f} &:= \frac{\partial f_z}{\partial z} + \frac{1}{r}\frac{\partial}{\partial r}(rf_r) + \frac{1}{r}\frac{\partial f_\phi}{\partial \phi},\\
\nabla f &:= \left[\frac{\partial f}{\partial z}, \frac{\partial f}{\partial r}, \frac{1}{r}\frac{\partial f}{\partial \phi}\right]^\top.
\end{aligned}$$

The steady state variant of the equations (6.1) defines a mapping $F : V \times \mathbb{R} \to V$, where $V = H^1(\Omega)^3 \times L_2(\Omega)$. Furthermore, the bounded linear operators

$$\begin{aligned}
\rho_\varphi \begin{pmatrix} u_r(r,\phi,z)\\ u_\phi(r,\phi,z)\\ u_z(r,\phi,z)\\ p(r,\phi,z)\end{pmatrix} &= \begin{pmatrix} u_r(r,\phi+\varphi,z)\\ u_\phi(r,\phi+\varphi,z)\\ u_z(r,\phi+\varphi,z)\\ p(r,\phi+\varphi,z)\end{pmatrix}, \quad \varphi\in[0,2\pi),\\
\rho_s \begin{pmatrix} u_r(r,\phi,z)\\ u_\phi(r,\phi,z)\\ u_z(r,\phi,z)\\ p(r,\phi,z)\end{pmatrix} &= \begin{pmatrix} u_r(r,-\phi,z)\\ -u_\phi(r,-\phi,z)\\ u_z(r,-\phi,z)\\ p(r,-\phi,z)\end{pmatrix}
\end{aligned}$$

are the image of the representation of the symmetry group $O(2)$ on the Hilbert space $V$. A straightforward calculation reveals that the operator $F$ is equivariant with respect to both $\rho_\varphi$ and $\rho_s$. Thus, we shall be concerned with investigating the stability of axisymmetric steady state solutions of (6.1); in this setting, we note that

$$u_\phi \equiv 0, \quad \partial u_z/\partial\phi \equiv 0, \quad \partial u_r/\partial\phi \equiv 0, \quad \partial p/\partial\phi \equiv 0.$$

Thereby, we need only consider the reduced problem: find $(\boldsymbol{u}^0, p^0) = (u_z^0, u_r^0, p^0) \in V^{O(2)}$ such that

$$\boldsymbol{\mathcal{L}}^0(\boldsymbol{u}^0, Re; p^0) \equiv \left\{ \begin{array}{rcl} \frac{1}{\mathrm{Re}}\nabla^2 u_z^0 + \nabla\cdot(u_z^0\mathbf{u}^0) - \frac{1}{2}(\nabla\cdot\boldsymbol{u}^0)u_z^0 + \frac{\partial p^0}{\partial z} &=& 0, \\ -\frac{1}{\mathrm{Re}}\left(\nabla^2 u_r^0 - \frac{u_r^0}{r^2}\right) + \nabla\cdot(u_r^0\mathbf{u}^0) - \frac{1}{2}(\nabla\cdot\boldsymbol{u}^0)u_r^0 + \frac{\partial p^0}{\partial r} &=& 0, \\ -\nabla\cdot\mathbf{u}^0 &=& 0. \end{array} \right. \tag{6.2}$$

Thus, in order to compute a solution belonging to $V^{O(2)}$, it is sufficient to only consider the domain $\Omega$ shown in Figure 6.2, which is a radial slice through the physical domain, subject to Dirichlet boundary conditions on $\Gamma_{\mathrm{in}}$ and $\Gamma_{\mathrm{wall}}$

$$u_z^0 = u_r^0 = 0 \text{ on } \Gamma_{\mathrm{wall}}, \tag{6.3}$$

$$u_r^0 = 0, \quad u_z^0 = g_d \text{ on } \Gamma_{\mathrm{in}}, \tag{6.4}$$

and natural boundary conditions on $\Gamma_{\mathrm{out}}$ and $\Gamma_{\mathrm{center}}$

$$\frac{\partial u_z^0}{\partial \mathbf{n}} - p^0 n_z = \frac{\partial u_r^0}{\partial \mathbf{n}} - p^0 n_r = 0 \text{ on } \Gamma_{\mathrm{out}} \cup \Gamma_{\mathrm{center}}. \tag{6.5}$$

We now linearize the Navier-Stokes equations (6.1) about the axisymmetric steady state solution $(\mathbf{u}^0, p^0)$, to obtain the following eigenvalue problem

$$\begin{aligned} -\frac{1}{\mathrm{Re}}\nabla^2 u_z^m + \nabla\cdot(u_z^m\mathbf{u}^0) + \nabla\cdot(u_z^0\mathbf{u}^m) - \frac{1}{2}\left((\nabla\cdot\boldsymbol{u}^m)u_z^0 + (\nabla\cdot\boldsymbol{u}^0)u_z^m\right) + \frac{\partial p^m}{\partial z} &= \lambda u_z^m, \\ -\frac{1}{\mathrm{Re}}\left(\nabla^2 u_r^m - \frac{u_r^m}{r^2} - \frac{2}{r^2}\frac{\partial u_\phi^m}{\partial \phi}\right) + \nabla\cdot(u_r^m\mathbf{u}^0) & \\ +\nabla\cdot(u_r^0\mathbf{u}^m) - \frac{1}{2}\left((\nabla\cdot\boldsymbol{u}^m)u_r^0 + (\nabla\cdot\boldsymbol{u}^0)u_r^m\right) + \frac{\partial p^m}{\partial r} &= \lambda u_r^m, \\ -\frac{1}{\mathrm{Re}}\left(\nabla^2 u_\phi^m - \frac{u_\phi^m}{r^2} - \frac{2}{r^2}\frac{\partial u_r^m}{\partial \phi}\right) + \nabla\cdot(u_\phi^m\mathbf{u}^0) & \\ +\frac{u_r^0 u_\phi^m}{r} - \frac{1}{2}(\nabla\cdot\boldsymbol{u}^0)u_\phi^m + \frac{1}{r}\frac{\partial p^m}{\partial \phi} &= \lambda u_\phi^m, \\ -\nabla\cdot\mathbf{u}^m &= 0, \end{aligned}$$

with boundary conditions

$$u_z^m = u_r^m = u_\phi^m = 0 \text{ on } \Gamma_{\mathrm{wall}}, \tag{6.6}$$

$$u_r^m = u_\phi^m = 0, \quad u_z = 0 \text{ on } \Gamma_{\mathrm{in}}, \tag{6.7}$$

$$\frac{\partial u_z^m}{\partial \mathbf{n}} - p n_z = \frac{\partial u_r^m}{\partial \mathbf{n}} - p n_r = \frac{\partial u_\phi^m}{\partial \mathbf{n}} - p n_\phi = 0 \text{ on } \Gamma_{\mathrm{out}} \cup \Gamma_{\mathrm{center}}. \tag{6.8}$$

The space $V$ can be decomposed into $O(2)$ invariant subspaces, *i.e.*,

$$V = \sum_{m=0}^{\infty} \oplus V^m,$$

where $V^0 = V^{O(2)}$, and for $m = 1, 2, \ldots$,

$$V^m = \mathrm{span}\left\{ \begin{pmatrix} u_z^m(z,r)\cos(m\phi) \\ u_r^m(z,r)\cos(m\phi) \\ u_\phi^m(z,r)\sin(m\phi) \\ p^m(z,r)\cos(m\phi) \end{pmatrix}, \begin{pmatrix} u_z^m(z,r)\sin(m\phi) \\ u_r^m(z,r)\sin(m\phi) \\ u_\phi^m(z,r)\cos(m\phi) \\ p^m(z,r)\sin(m\phi) \end{pmatrix} \right\}.$$

We remark that

$$V^{m,s} = \text{span}\left\{ \begin{pmatrix} u_z^m(x,r)\cos(m\phi) \\ u_r^m(x,r)\cos(m\phi) \\ u_\phi^m(x,r)\sin(m\phi) \\ p^m(x,r)\cos(m\phi) \end{pmatrix} \right\} \text{ and } \mathrm{V^{m,a}} = \text{span}\left\{ \begin{pmatrix} u_z^m(x,r)\sin(m\phi) \\ u_r^m(x,r)\sin(m\phi) \\ u_\phi^m(x,r)\cos(m\phi) \\ p^m(x,r)\sin(m\phi) \end{pmatrix} \right\},$$

$m = 1, 2, \ldots$, are symmetric and antisymmetric subspaces of $V^m$, respectively. Thus, bearing in mind (3.7), we can seek to find $(\mathbf{u}^m, p^m) \in V^{m,s}$ or $V^{m,a}$, $m = 1, 2, \ldots$, and a straightforward calculation leads us to the following set of eigenvalue equations

$$\boldsymbol{\mathcal{L}}^m(\boldsymbol{u}^0, Re; \boldsymbol{u}^m, p^m) \equiv \left\{ \begin{array}{rcl} -\frac{1}{\mathrm{Re}}\nabla_2^2 u_z^m + \nabla_2 \cdot (u_z^m \mathbf{u}_{z.r}^0) + \nabla_2 \cdot (u_z^0 \mathbf{u}_{z.r}^m) & & \\ -\frac{1}{2}\left( (\nabla_2 \cdot \boldsymbol{u}_{z.r}^m + \frac{m}{r} u_\phi^m) u_z^0 + (\nabla_2 \cdot \boldsymbol{u}_{z.r}^0) u_z^m \right) & & \\ \qquad + \frac{m}{r} u_z^0 u_\phi^m + \frac{\partial p^m}{\partial z} & = & \lambda u_z^m, \\ -\frac{1}{\mathrm{Re}}[\nabla_2^2 u_r^m - \frac{u_r^m}{r^2} - \frac{2m}{r^2} u_\phi^m] + \nabla_2 \cdot (u_r^m \mathbf{u}_{z.r}^0) & & \\ -\frac{1}{2}\left( (\nabla_2 \cdot \boldsymbol{u}_{z.r}^m + \frac{m}{r} u_\phi^m) u_r^0 + (\nabla_2 \cdot \boldsymbol{u}_{z.r}^0) u_r^m \right) & & \\ \qquad + \nabla_2 \cdot (u_r^0 \mathbf{u}_{z.r}^m) + \frac{m}{r} u_r^0 u_\phi^m + \frac{\partial p^m}{\partial r} & = & \lambda u_r^m, \\ -\frac{1}{\mathrm{Re}}[\nabla_2^2 u_\phi^m - \frac{u_\phi^m}{r^2} - \frac{2m}{r^2} u_r^m] + \nabla_2 \cdot (u_\phi^m \mathbf{u}_{z.r}^0) & & \\ \qquad + \frac{u_r^0 u_\phi^m}{r} - \frac{1}{2}(\nabla_2 \cdot \boldsymbol{u}_{z.r}^0) u_\phi^m - \frac{m}{r} p^m & = & \lambda u_\phi^m, \\ -\nabla_2 \cdot (\mathbf{u}_{z.r}^m) - \frac{m}{r} u_\phi^m & = & 0, \end{array} \right. \tag{6.9}$$

where $\mathbf{f}_{z.r} := [f_z, f_r]^\top$ and

$$\nabla_2^2 f := \frac{\partial^2 f}{\partial z^2} + \frac{1}{r}\frac{\partial}{\partial r}\left( r \frac{\partial f}{\partial r} \right) - \frac{m^2}{r^2} f, \qquad \nabla_2 \cdot \mathbf{f}_{z.r} := \frac{\partial f_z}{\partial z} + \frac{1}{r}\frac{\partial}{\partial r}(r f_r).$$

Here, we notice that for each $m = 1, 2, \ldots$, the dependency on the azimuthal angle $\phi$ has been removed and hence the original three–dimensional eigenvalue problem has been reduced to a series of two–dimensional ones which can be solved on the same domain $\Omega$ as used for the axisymmetric steady state solution, albeit we now have 4 unknowns, rather than the 3 we had before. Thus, for a specific Reynolds number $Re^0$, the eigenvalues and eigenvectors can be approximated by solving the system: find the triples $\{(\boldsymbol{u}^0, p^0), (\boldsymbol{u}^m, p^m), \mu^0\} \in V^0 \times V^{m,s} \times \mathbb{R}$, $m = 1, 2, \ldots$, satisfying

$$\begin{pmatrix} \boldsymbol{\mathcal{L}}^0(\boldsymbol{u}^0, Re^0; p^0) \\ \boldsymbol{\mathcal{L}}^m(\boldsymbol{u}^0, Re^0; \boldsymbol{u}^m, p^m) - \mu^0 \hat{\mathbf{u}}^m \end{pmatrix} = \mathbf{0}, \tag{6.10}$$

where $\hat{\mathbf{u}}^m = (u_z^m, u_r^m, u_\phi^m, 0)^\top$, subject to boundary conditions (6.3)–(6.5), (6.6)–(6.8). Finally, the location of critical bifurcation points can be determined by solving the following extended system: find the triple $\{(\boldsymbol{u}^0, p^0), (\boldsymbol{u}^m, p^m), Re^0\} \in V^0 \times V^{m,s} \times \mathbb{R}$, $m = 1, 2, \ldots$, such that

$$\begin{pmatrix} \boldsymbol{\mathcal{L}}^0(\boldsymbol{u}^0, Re^0; p^0) \\ \boldsymbol{\mathcal{L}}^m(\boldsymbol{u}^0, Re^0; \boldsymbol{u}^m, p^m) \\ (\boldsymbol{u}^m, g) - 1 \end{pmatrix} = 0, \tag{6.11}$$

subject to boundary conditions (6.3)–(6.5), (6.6)–(6.8).

**6.2. Meshes and traces.** In this section we introduce the notation needed to define the interior penalty DG discretization of the primal problems (6.10) and (6.11) subject to the boundary conditions (6.3)–(6.5), (6.6)–(6.8).

To this end, we assume that $\Omega \subset \mathbb{R}^2$ can be subdivided into shape-regular meshes $\mathcal{T}_h = \{\kappa\}$ consisting of elements $\kappa$ which are either triangles or quadrilaterals. For each $\kappa \in \mathcal{T}_h$, we denote by $\mathbf{n}_\kappa$ the unit outward normal vector to the boundary $\partial\kappa$, and by $h_\kappa$ the elemental diameter. An interior edge of $\mathcal{T}_h$ is the (non-empty) one-dimensional interior of $\partial\kappa^+ \cap \partial\kappa^-$, where $\kappa^+$ and $\kappa^-$ are two adjacent elements of $\mathcal{T}_h$. Similarly, a boundary edge of $\mathcal{T}_h$ is the (non-empty) one-dimensional interior of $\partial\kappa \cap \Gamma$ which consists of entire edges of $\partial\kappa$. We denote by $\Gamma_{\text{int}}$ the union of all interior edges of $\mathcal{T}_h$.

Next, we define average and jump operators. To this end, let $\kappa^+$ and $\kappa^-$ be two adjacent elements of $\mathcal{T}_h$, and $\mathbf{x}$ be an arbitrary point on the interior edge $e = \partial\kappa^+ \cap \partial\kappa^- \subset \Gamma_{\text{int}}$. Furthermore, let $q$, $\mathbf{v}$, and $\underline{\tau}$ be scalar–, vector–, and matrix–valued functions, respectively, that are smooth inside each element $\kappa^\pm$. By $(q^\pm, \mathbf{v}^\pm, \underline{\tau}^\pm)$ we denote the traces of $(q, \mathbf{v}, \underline{\tau})$ on $e$ taken from within the interior of $\kappa^\pm$, respectively. Then, we introduce the following averages at $\mathbf{x} \in e$:

$$\{\!\{q\}\!\} = (q^+ + q^-)/2, \quad \{\!\{\mathbf{v}\}\!\} = (\mathbf{v}^+ + \mathbf{v}^-)/2, \quad \{\!\{\underline{\tau}\}\!\} = (\tau^+ + \tau^-)/2.$$

Similarly, the jumps at $\mathbf{x} \in e$ are given by

$$\begin{aligned} [\![q]\!] &= q^+\mathbf{n}_{\kappa^+} + q^-\mathbf{n}_{\kappa^-}, \quad [\![\mathbf{v}]\!] = \mathbf{v}^+ \cdot \mathbf{n}_{\kappa^+} + \mathbf{v}^- \cdot \mathbf{n}_{\kappa^-}, \\ \underline{[\![\mathbf{v}]\!]} &= \mathbf{v}^+ \otimes \mathbf{n}_{\kappa^+} + \mathbf{v}^- \otimes \mathbf{n}_{\kappa^-}, \quad [\![\underline{\tau}]\!] = \underline{\tau}^+\mathbf{n}_{\kappa^+} + \underline{\tau}^-\mathbf{n}_{\kappa^-}. \end{aligned}$$

On boundary edges $e \subset \Gamma$, we set $\{\!\{q\}\!\} = q$, $\{\!\{\mathbf{v}\}\!\} = \mathbf{v}$, $\{\!\{\underline{\tau}\}\!\} = \underline{\tau}$, $[\![q]\!] = q\mathbf{n}$, $[\![\mathbf{v}]\!] = \mathbf{v} \cdot \mathbf{n}$, $\underline{[\![\mathbf{v}]\!]} = \mathbf{v} \otimes \mathbf{n}$, and $[\![\underline{\tau}]\!] = \underline{\tau}\mathbf{n}$. Here, $\mathbf{n}$ is the unit outward normal vector to the boundary $\Gamma$. For matrices $\underline{\sigma}$, $\underline{\tau} \in \mathbb{R}^{m\times n}$, $m, n \geq 1$, we use the standard notation $\underline{\sigma} : \underline{\tau} = \sum_{k=1}^m \sum_{l=1}^n \sigma_{kl}\tau_{kl}$.

**6.3. Discontinuous Galerkin discretization.** We now present the DG discretization employed for the numerical approximation of the eigenvalue problem (6.10) and bifurcation problem (6.11)), together with the associated boundary conditions (6.3)–(6.5), (6.6)–(6.8). To this end, for a given mesh $\mathcal{T}_h$ and polynomial degree $k \geq 1$, we introduce the following finite element spaces

$$\begin{aligned} \mathbf{V}^0_{h,k} &= \{\mathbf{v} \in [L^2(\Omega)]^2 : \mathbf{v}|_\kappa \in [\mathcal{R}^k(\kappa)]^2, \kappa \in \mathcal{T}_h\}, \\ \mathbf{V}^m_{h,k} &= \{\mathbf{v} \in [L^2(\Omega)]^3 : \mathbf{v}|_\kappa \in [\mathcal{R}^k(\kappa)]^3, \kappa \in \mathcal{T}_h\}, \\ Q_{h,k} &= \{q \in L^2(\Omega) : q|_\kappa \in \mathcal{R}^{k-1}(\kappa), \kappa \in \mathcal{T}_h\}, \end{aligned}$$

where, $\mathcal{R}^k(\kappa)$ is $\mathcal{P}^p(\kappa)$ when $\kappa$ is a triangle and $\mathcal{R}^k(\kappa)$ is $\mathcal{Q}^k(\kappa)$ when $\kappa$ is a quadrilateral. Here, $\mathcal{P}^k(\kappa)$ denotes the set of polynomials of total degree $k$ on $\kappa$, while $\mathcal{Q}^k(\kappa)$ denotes the set of all tensor-product polynomials on $\kappa$ of degree $k$ in each coordinate direction. Finally, we let

$$\mathbf{V}_{h,k} := (\mathbf{V}^0_{h,k} \times Q_{h,k}) \times (\mathbf{V}^m_{h,k} \times Q_{h,k}) \times \mathbb{R}, \quad m = 1, 2, \ldots.$$

We now introduce the following symmetric version of the interior penalty method, together with a Lax-Friedrichs numerical flux approximation of the nonlinear convective terms. For the eigenvalue problem we seek to find $\boldsymbol{u}_h = \{(\boldsymbol{u}^0_h, p^0_h), (\boldsymbol{u}^m_h, p^m_h), \mu^0_h\} \in \mathbf{V}_{h,k}$, $m = 1, 2, \ldots$, such that

$$\left\{ \begin{array}{lcc} A_h(\mathbf{u}^0_h, Re^0_h, \mathbf{v}^0_h) + C_h(\mathbf{u}^0_h; \mathbf{v}^0_h) + B_h(\mathbf{v}^0_h, p^0_h) & = & \ell_1(Re^0_h; \mathbf{v}^0_h), \\ B_h(\mathbf{u}^0_h, q^0_h) & = & \ell_2(q^0_h), \\ \hat{A}_h(\mathbf{u}^0_h, Re^0_h\mathbf{v}^m_h) + \hat{C}_h(\mathbf{u}^0_h; \mathbf{u}^m_h, \mathbf{v}^m_h) + \hat{B}_h(\mathbf{v}^m_h, p^m_h) & = & \mu^0_h(\mathbf{u}^m_h, \mathbf{v}^m_h), \\ \hat{B}_h(\mathbf{u}^m_h, q^m_h) & = & 0, \end{array} \right\} \quad (6.12)$$

for all $\mathbf{v}_h := \{(\mathbf{v}_h^0, q_h^0), (\mathbf{v}_h^m, q_h^m), \chi_h\} \in \mathbf{V}_{h,k}$. Similarly, to locate a steady bifurcation point we solve: find $\boldsymbol{u}_h = \left\{(\boldsymbol{u}_h^0, p_h^0), (\boldsymbol{u}_h^m, p_h^m), Re_h^0\right\} \in \mathbf{V}_{h,k}$, $m = 1, 2, \ldots$, such that

$$\left\{\begin{array}{lcc} A_h(\mathbf{u}_h^0, Re_h^0, \mathbf{v}_h^0) + C_h(\mathbf{u}_h^0; \mathbf{v}_h^0) + B_h(\mathbf{v}_h^0, p_h^0) & = & \ell_1(Re_h^0; \mathbf{v}_h^0), \\ B_h(\mathbf{u}_h^0, q_h^0) & = & \ell_2(q_h^0), \\ \hat{A}_h(\mathbf{u}_h^0, Re_h^0, \mathbf{v}_h^m) + \hat{C}_h(\mathbf{u}_h^0; \mathbf{u}_h^m, \mathbf{v}_h^m) + \hat{B}_h(\mathbf{v}_h^m, p_h^m) & = & 0, \\ \hat{B}_h(\mathbf{u}_h^m, q_h^m) & = & 0, \\ \chi_h(\mathbf{u}_h^m, g) & = & 1, \end{array}\right. \tag{6.13}$$

for all $\mathbf{v}_h := \{(\mathbf{v}_h^0, q_h^0), (\mathbf{v}_h^m, q_h^m), \chi_h\} \in \mathbf{V}_{h,k}$. Here, the bilinear forms $A_h$, $\hat{A}_h$, $B_h$ and $\hat{B}_h$ are defined, respectively, by

$$\begin{aligned} A_h(\mathbf{u}, Re, \mathbf{v}) = \frac{1}{\mathrm{Re}} \Bigg( & \int_\Omega \nabla_h \mathbf{u} : \nabla_h \mathbf{v} \, \mathrm{d}\mathbf{x} + \int_\Omega \frac{u_r}{r^2} v_r \, \mathrm{d}\mathbf{x} \\ & - \int_{\Gamma_{\mathrm{int}} \cup \Gamma_{\mathrm{in}}} (\{\!\{\nabla_h \mathbf{v}\}\!\} : \underline{[\![\mathbf{u}]\!]} + \{\!\{\nabla_h \mathbf{u}\}\!\} : \underline{[\![\mathbf{v}]\!]}) \, \mathrm{d}s \\ & + \int_{\Gamma_{\mathrm{int}} \cup \Gamma_{\mathrm{in}}} \sigma \underline{[\![\mathbf{u}]\!]} : \underline{[\![\mathbf{v}]\!]} \, \mathrm{d}s \Bigg) \\ \hat{A}_h(\mathbf{u}, Re, \mathbf{v}) = \frac{1}{\mathrm{Re}} \Bigg( & \int_\Omega \nabla_h \mathbf{u} : \nabla_h \mathbf{v} \, \mathrm{d}\mathbf{x} + \int_\Omega \frac{m^2}{r^2} \mathbf{u} \cdot \mathbf{v} \, \mathrm{d}\mathbf{x} \\ & + \int_\Omega \left( \frac{u_r}{r^2} + \frac{2m}{r^2} u_\phi^m \right) v_r \, \mathrm{d}\mathbf{x} + \int_\Omega \left( \frac{u_\phi}{r^2} + \frac{2m}{r^2} u_r^m \right) v_\phi \, \mathrm{d}\mathbf{x} \\ & - \int_{\Gamma_{\mathrm{int}} \cup \Gamma_{\mathrm{in}}} (\{\!\{\nabla_h \mathbf{v}\}\!\} : \underline{[\![\mathbf{u}]\!]} + \{\!\{\nabla_h \mathbf{u}\}\!\} : \underline{[\![\mathbf{v}]\!]}) \, \mathrm{d}s \\ & + \int_{\Gamma_{\mathrm{int}} \cup \Gamma_{\mathrm{in}}} \sigma \underline{[\![\mathbf{u}]\!]} : \underline{[\![\mathbf{v}]\!]} \, \mathrm{d}s \Bigg) \\ B_h(\mathbf{v}, q) = & - \int_\Omega q \nabla_h \cdot \mathbf{v} \, \mathrm{d}\mathbf{x} + \int_{\Gamma_{\mathrm{int}} \cup \Gamma_{\mathrm{in}}} \{\!\{q\}\!\} [\![\mathbf{v}]\!] \, \mathrm{d}s, \\ \hat{B}_h(\mathbf{v}, q) = & - \int_\Omega q \nabla_{2,h} \cdot \mathbf{v}_{z.r} \, \mathrm{d}\mathbf{x} - \int_\Omega \frac{m}{r} q v_\phi \, \mathrm{d}\mathbf{x} \\ & + \int_{\Gamma_{\mathrm{int}} \cup \Gamma_{\mathrm{in}}} \{\!\{q\}\!\} [\![\mathbf{v}_{z.r}]\!] \, \mathrm{d}s, \end{aligned}$$

where the operator $\boldsymbol{\nabla}_h$ is used to denote the broken gradient operator $\boldsymbol{\nabla}$, defined elementwise. The function $\sigma \in L^\infty(\Gamma_{\mathrm{int}} \cup \Gamma)$ is the so–called interior penalty function, which is chosen as follows: writing $\mathrm{h} \in L^\infty(\Gamma_{\mathrm{int}} \cup \Gamma)$ to denote the mesh function defined by

$$\mathrm{h}(\mathbf{x}) = \left\{\begin{array}{ll} \min\{h_\kappa, h_{\kappa'}\}, & \mathbf{x} \in e = \partial\kappa \cap \partial\kappa' \subset \Gamma_{\mathrm{int}}, \\ h_\kappa, & \mathbf{x} \in e = \partial\kappa \cap \Gamma, \end{array}\right.$$

we set

$$\sigma = C_\sigma \frac{k^2}{\mathrm{h}}.$$

Here, $C_\sigma$ is a positive constant which is independent of the mesh size and the polynomial degree $k$. To guarantee stability of the bilinear forms $A_h$ and $\hat{A}_h$, $C_\sigma$ must be chosen sufficiently large; see [4], for example, and the references cited therein.

The semilinear form $C_h$ represents the approximation of the nonlinear convection terms and is defined by

$$C_h(\mathbf{u},\mathbf{v}) = -\int_\Omega \mathcal{F}^0(\boldsymbol{u}) : \nabla_h \mathbf{v}\,\mathrm{d}\mathbf{x} - \frac{1}{2}\int_\Omega (\nabla_h\cdot\boldsymbol{u})\boldsymbol{u}\cdot\boldsymbol{v}\,\mathrm{d}\boldsymbol{x} + \sum_{\kappa\in\mathcal{T}_h}\left(\int_{\partial\kappa\setminus\Gamma}\mathcal{H}(\mathbf{u}^+,\mathbf{u}^-,\mathbf{n})\cdot\mathbf{v}^+\,\mathrm{d}s + \int_{\partial\kappa\cap\Gamma}\mathcal{H}(\mathbf{u}^+,\mathbf{u}_\Gamma(\mathbf{u}),\mathbf{n})\cdot\mathbf{v}^+\,\mathrm{d}s\right),$$

where $\mathcal{H}(\cdot,\cdot,\cdot)$ denotes the Lax-Friedrichs flux given by

$$\mathcal{H}(\boldsymbol{v},\boldsymbol{w},\boldsymbol{n}) := \frac{1}{2}\left(\mathcal{F}^0(\boldsymbol{v})\cdot\boldsymbol{n} + \mathcal{F}^0(\boldsymbol{w})\cdot\boldsymbol{n} - \alpha(\boldsymbol{w}-\boldsymbol{v})\right). \tag{6.14}$$

Here,

$$\mathcal{F}^0(\mathbf{u}^0) := \mathbf{u}^0\otimes\mathbf{u}^0$$

and $\alpha := \max(\mu^+,\mu^-)$, where $\mu^+$ and $\mu^-$ are the largest eigenvalues (in absolute magnitude) of the Jacobi matrices $(\partial/\partial\mathbf{u})(\mathcal{F}^0(\cdot)\cdot\mathbf{n})$ evaluated at $\mathbf{v}$ and $\mathbf{w}$, respectively. Thereby, in this setting, we have $\alpha = 2\max(|\mathbf{v}\cdot\mathbf{n}|,|\mathbf{w}\cdot\mathbf{n}|)$.

The boundary function $\boldsymbol{u}_\Gamma$ is given according to the type of boundary condition imposed. To this end, we set

$$\mathcal{H}(\mathbf{u},\mathbf{w},\mathbf{n}) := \frac{1}{2}\left(\begin{bmatrix} u_z\mathbf{u}\cdot\mathbf{n} \\ u_r\mathbf{u}\cdot\mathbf{n}\end{bmatrix} + \begin{bmatrix} w_z\mathbf{w}\cdot\mathbf{n} \\ w_r\mathbf{w}\cdot\mathbf{n}\end{bmatrix} + \alpha(\mathbf{u}-\mathbf{w})\right)$$

and $\alpha := \max(\alpha_\mathbf{u},\alpha_\mathbf{w})$, where $\alpha_\mathbf{u}$ is the eigenvalue with largest magnitude of the Jacobi matrix

$$\frac{\partial}{\partial\mathbf{u}}\begin{bmatrix} u_z\mathbf{u}\cdot\mathbf{n} \\ u_r\mathbf{u}\cdot\mathbf{n}\end{bmatrix}.$$

In our case $\alpha_\mathbf{u} = |2\mathbf{u}\cdot\mathbf{n}|$. Finally, the boundary function $\mathbf{u}_\Gamma$ is given by

$$\mathbf{u}_\Gamma(\mathbf{u}) = [g_d,0]^\top \text{ on } \Gamma_{\text{in}}, \quad \mathbf{u}_\Gamma(\mathbf{u}) = \mathbf{0} \text{ on } \Gamma_{\text{wall}},$$

$$\mathbf{u}_\Gamma(\mathbf{u}) = \mathbf{u} \text{ on } \Gamma_{\text{out}}\cup\Gamma_{\text{center}}.$$

In a similar way, $\hat{C}_h$ represents the approximation of the linearization of the convection terms. Integration by parts and a further application of the Lax-Friedrichs flux gives

$$\begin{aligned}\hat{C}_h(\mathbf{u}^m,\mathbf{v};\mathbf{u}^0) = &-\int_\Omega\left((\mathbf{u}^m\otimes\mathbf{u}^0_{z.r}) : \nabla_h\mathbf{v} + (\mathbf{u}^0_{z.r}\otimes\mathbf{u}^m_{z.r}) : \nabla_h\bar{\mathbf{v}}_{z.r}\right)\mathrm{d}\mathbf{x}\\ &+\int_\Omega\left(\frac{m}{r}u^m_\phi\mathbf{u}^0_{z.r}\cdot\bar{\mathbf{v}}_{z.r} + \frac{u^0_r u^m_\phi}{r}\bar{v}_\phi\right)\mathrm{d}\mathbf{x}\\ &+\sum_{\kappa\in\mathcal{T}_h}\left(\int_{\partial\kappa\setminus\Gamma}\hat{\mathcal{H}}(\mathbf{u}^{m,+},\mathbf{u}^{m,-},\mathbf{n};(\mathbf{u}^{0,+}+\mathbf{u}^{0,-})/2)\cdot\bar{\mathbf{v}}^+\,\mathrm{d}s\right.\\ &\left.+\int_{\partial\kappa\cap\Gamma}\hat{\mathcal{H}}(\mathbf{u}^{m,+},\hat{\mathbf{u}}_\Gamma(\mathbf{u}^m),\mathbf{n};(\mathbf{u}^{0,+}+\mathbf{u}_\Gamma(\mathbf{u}^0))/2)\cdot\mathbf{v}^+\,\mathrm{d}s\right),\end{aligned}$$

where

$$\hat{\mathcal{H}}(\mathbf{u},\mathbf{w},\mathbf{n};\mathbf{v}) := \frac{1}{2}\left( \begin{bmatrix} (u_z\mathbf{v}_{z.r} + v_z\mathbf{u}_{z.r})\cdot\mathbf{n} \\ (u_r\mathbf{v}_{z.r} + v_r\mathbf{u}_{z.r})\cdot\mathbf{n} \\ u_\phi\mathbf{v}_{z.r}\cdot\mathbf{n} \end{bmatrix} + \begin{bmatrix} (w_z\mathbf{v}_{z.r} + v_z\mathbf{w}_{z.r})\cdot\mathbf{n} \\ (w_r\mathbf{v}_{z.r} + v_r\mathbf{w}_{z.r})\cdot\mathbf{n} \\ w_\phi\mathbf{v}_{z.r}\cdot\mathbf{n} \end{bmatrix} + \hat{\alpha}(\mathbf{u}-\mathbf{w}) \right).$$

In this case $\hat{\alpha} = |2\mathbf{v}_{z.r}\cdot\mathbf{n}|$, $\mathbf{u}_\Gamma$ is as defined above, while $\hat{\mathbf{u}}_\Gamma$ is given by

$$\hat{\mathbf{u}}_\Gamma(\mathbf{u}) = \mathbf{0} \text{ on } \Gamma_{\text{in}}, \quad \hat{\mathbf{u}}_\Gamma(\mathbf{u}) = \mathbf{0} \text{ on } \Gamma_{\text{wall}},$$

$$\hat{\mathbf{u}}_\Gamma(\mathbf{u}) = \mathbf{u} \text{ on } \Gamma_{\text{out}} \cup \Gamma_{\text{center}}.$$

Finally, $\ell_1(\cdot;\cdot)$ and $\ell_2(\cdot)$ are given respectively by

$$\ell_1(Re;\mathbf{v}) = -\frac{1}{Re}\int_{\Gamma_{\text{D}}} ((\mathbf{g}_{\text{D}}\otimes\mathbf{n}) : \nabla\mathbf{v} - \sigma\mathbf{g}_{\text{D}}\cdot\mathbf{v})\, \mathrm{d}s,$$
$$\ell_2(q) = \int_{\Gamma_{\text{D}}} q\mathbf{g}_{\text{D}}\cdot\mathbf{n}\, \mathrm{d}s. \tag{6.15}$$

**7. Numerical Experiments.** In this section we first present two numerical examples to demonstrate the practical performance of the proposed *a posteriori* error estimator derived in Section 4 within an automatic adaptive refinement procedure which is based on employing 1-irregular quadrilateral elements. Here, the elements are marked for refinement/derefinement on the basis of the size of the elemental error indicators $|\eta_\kappa|$, using the fixed fraction refinement algorithm with refinement and derefinement fractions set to 25% and 10%, respectively. Then, in the third example we present results for the cylindrical pipe with a sudden expansion, where we use both the error estimate derived in Section 4 and the error estimate for the eigenvalues, see [11]. In this case we compare the numerical results with recent experimental data, see Mullin *et al.* [25]. In each of the examples shown in this section, we set $C_\sigma = 10$, $p = 2$, and $\hat{p} = 3$.

Throughout this section, the underlying linear systems are solved using the MUltifrontal Massively Parallel Solver, see [1, 2, 3] for details. In order to obtain the initial guess for the damped Newton method, once a base solution has been obtained for a specific Reynolds number, we employ the Arnoldi Package (ARPACK) of Lehoucq, Sorensen and Yang [24] to calculate the most dangerous eigenvalue and corresponding eigenfunctions. ARPACK is most adept at finding highly separated eigenvalues with large magnitude and not necessarily those with small real part that determine linear stability. To overcome this difficulty we employ the modified Cayley transform outlined in Cliffe *et al.* [9], for example.

**7.1. Example 1.** In our first example we consider a cylindrical pipe of diameter D with an axisymmetric stenotic region of axial length $L$ and radius $r(x)$, given by

$$r(z) = (D_{\min} + (D - D_{\min})\sin^2(\pi z L))/2, \quad -1/2 \le z/L \le 1/2,$$

where $z$ denotes the coordinate direction along the pipe, centered in the middle of the stenosis, see Figure 7.1. Writing $S$ to denote the stenosis degree, defined, by

$$S = 1 - (D_{\min}/D)^2,$$

we consider the geometry specified by $S = 0.75$, with the stenosis length $L/D$ equal to 2. This problem has been considered recently by Sherwin & Blackburn [26], Blackburn

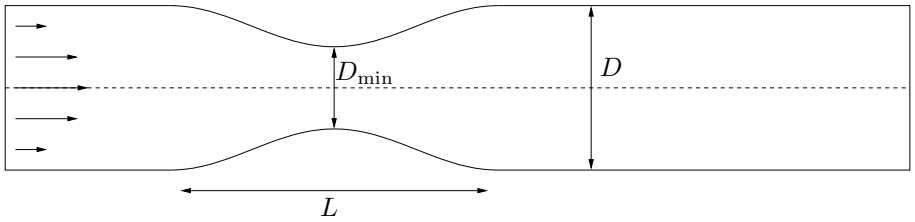


FIG. 7.1. *Example 1: Stenosis domain.*

| No. Eles | Base DOF | Null DOF | $Re_h^0$ | $\lvert Re^0 - Re_h^0\rvert$ | $\lvert\sum_{\kappa\in\mathcal{T}_h}\eta_\kappa\rvert$ | $\tau$ |
|---|---|---|---|---|---|---|
| 3840 | 84480 | 119040 | 688.07858 | 32.974 | 27.337 | 0.83 |
| 6771 | 148962 | 209901 | 717.87440 | 3.178 | 3.629 | 1.14 |
| 11754 | 258588 | 364374 | 720.31797 | 7.348E-01 | 7.739E-01 | 1.05 |
| 20265 | 445830 | 628215 | 720.82707 | 2.257E-01 | 2.280E-01 | 1.01 |
| 35064 | 771408 | 1086984 | 720.93597 | 1.168E-01 | 1.168E-01 | 1.00 |
| 60678 | 1334916 | 1881018 | 720.97594 | 7.677E-02 | 7.677E-02 | 1.00 |

TABLE 7.1
*Example 1: Performance of the adaptive algorithm.*

*et al.* [7] and also as a test problem in Cliffe *et al.* [11]. In this setting, with a Poiseuille flow profile at the inlet, a steady $O(2)$ symmetry breaking occurs with azimuthal wave number $m = 1$ when $Re^0 = 721.05272346$ to 8 decimal places. We use an initial mesh fitted to the stenosis with 3840 elements, which is long enough to ensure Poiseuille flow has redeveloped at the outlet of the pipe, and carry out 5 adaptive refinement steps using the fixed fraction refinement strategy. To this end, Table 7.1 shows the number of elements, the number of degrees of freedom in computing the primal base solution and the primal null function, the computed critical Reynolds number $Re_h^0$, the error in the critical Reynolds number, the computed error representation formula $\lvert\sum_{\kappa\in\mathcal{T}_h}\eta_\kappa\rvert$ and the resulting effectivity indices $\tau = \lvert\sum_{\kappa\in\mathcal{T}_h}\eta_\kappa\rvert/\lvert Re^0 - Re_h^0\rvert$. We notice immediately that, as the mesh is refined, the effectivity indices tend to unity, indicating that our error indicator is performing extremely well. Figures 7.2(a) and 7.2(b) show the resultant mesh and a close up of the mesh near the stenosis, respectively, after 5 adaptive refinement steps. We notice that refinement has been carried out primarily downstream from the stenosis near the wall of the pipe, although some further refinement has also been performed upstream from the stenosis.

Finally, in Figure 7.3 we show a comparison of the adaptive refinement strategy with a uniform mesh refinement algorithm; here the error in the computed critical Reynolds number is plotted against the number of degrees of freedom (in the primal base problem) for both strategies. We see immediately that the adaptive refinement strategy is superior to uniform refinement, in the sense that, for a given number of degrees of freedom, the error in the critical Reynolds number is always less than the corresponding quantity computed using simply uniform refinement of the mesh. Indeed, on the final grid we notice around an order of magnitude reduction in the error when the former strategy is employed.

**7.2. Example 2.** In our second example we consider a cylindrical pipe, of radius $R_1$, blocked by a sphere, of radius $R_2$, centered on the axis of symmetry of the pipe. Here, we shall be interested in an axisymmetric steady solution and hence we can

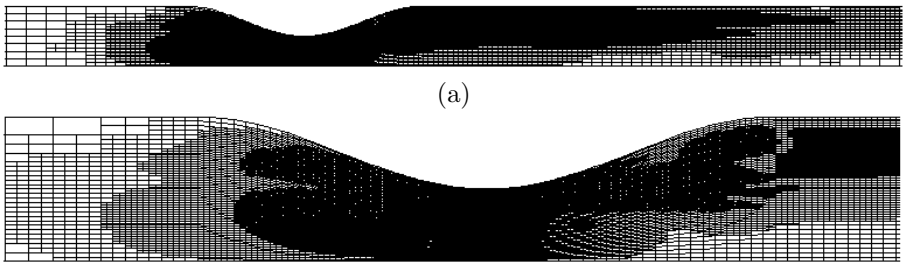

(a)

(b)

FIG. 7.2. *Example 1: (a) Mesh after 5 refinement steps; (b) Mesh detail.*

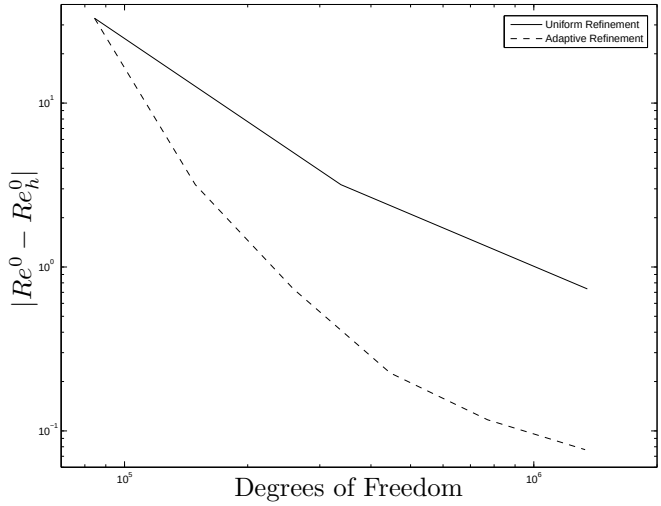


FIG. 7.3. *Example 1: Convergence of the error in the approximation of the critical* $Re^0$.

use the two–dimensional domain shown in Figure 7.4 to calculate the base flow; we choose $R_1 : R_2 = 2 : 1$. Computations on a fine grid reveals that the symmetric steady solution becomes unstable at the critical Reynolds number $Re^0 = 359.366955598$. We use an initial mesh fitted to the blockage, with 2032 elements and carry out 5 adaptive refinement steps using the fixed fraction refinement strategy outlined above.

The performance of the proposed adaptive algorithm is presented in Table 7.2. shows the effectivities for the error indicator, $|\sum_{\kappa\in\mathcal{T}_h}\eta_\kappa|$. As before, we show in tabular form the number of elements, the number of degrees of freedom for both the primal base and primal null solutions, the computed critical Reynolds number $Re_h^0$, the error in the critical Reynolds number, the computed error representation formula, and the effectivity indices $\tau = |\sum_{\kappa\in\mathcal{T}_h}\eta_\kappa|/|Re^0 - Re_h^0|$. In this case, we again observe that the effectivity indices tend to unity as the mesh is refined; indeed, the effectivities are very close to 1 after only 2 refinement steps. Plots of the mesh after 5 refinements are shown in Figures 7.5(a) and 7.6, the first showing the entire mesh, while the second shows the mesh detail near the blockage. We notice that a significant amount of refinement has been carried out upstream of the blockage (although more has been

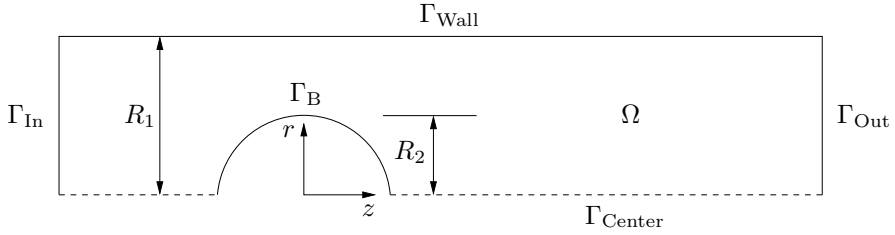


FIG. 7.4. *Example 2: Half Channel with a Cylindrical Blockage.*

| No. Elements | Base DOF | Null DOF | $Re_h^0$ | $\lvert Re^0 - Re_h^0 \rvert$ | $\tau$ |
|---|---|---|---|---|---|
| 2032 | 44704 | 62992 | 528.851 | 1.695E+02 | 2.097 |
| 3589 | 78958 | 111259 | 362.989 | 3.622 | 1.193 |
| 6265 | 137830 | 194215 | 359.748 | 3.815E-01 | 0.833 |
| 10987 | 241714 | 340597 | 359.401 | 3.452E-02 | 0.941 |
| 19681 | 432982 | 610111 | 359.387 | 2.042E-02 | 0.960 |
| 34948 | 768856 | 1083388 | 359.365 | 2.234E-03 | 1.000 |

TABLE 7.2
*Example 2: Performance of the adaptive algorithm.*

performed downstream); this is possibly in response to the structure in the radial component of the primal base solution, cf. Figure 7.5(b).

Finally, Figure 7.7 presents a comparison of the error in the computed critical Reynolds number employing both the proposed adaptive refinement strategy and uniform mesh refinement. As with the previous example, the adaptive strategy shows a great improvement in the error in the computed critical Reynolds number in comparison to the same quantity computed using uniform refinement; indeed, on the final mesh, we witness around two orders of magnitude improvement in error when the adaptive strategy is employed.

**7.3. Example 3.** Our final example concerns the stability of axisymmetric flows in a cylindrical pipe with a sudden expansion, with inlet to outlet ratio of $R_1 : R_2$, see Figure 7.8. At the inlet we assume Poiseuille flow. Recent experimental work, for the case $R_1 : R_2 = 1 : 2$, has revealed that a steady symmetric flow becomes asymmetric at Reynolds number $Re^0 = 1139 \pm 10$, and the resulting steady asymmetric flow is stable until the onset of time dependence at $Re^0 = 1453 \pm 41$, see [25].

We begin by investigating the nature of the 'most dangerous' eigenvalues for the problem $R_2/R_1 = 2$ for a series of Reynolds number from $Re = 600$ to $Re = 1600$, for the modes $m = 1, \ldots, 4$, all calculations being performed on a mesh consisting of 20000 elements graded toward the expansion. Here, the computational domain is sufficiently long to ensure Poiseuille flow has redeveloped at the outlet (in this case 400 pipe radii long). From Figure 7.9 we notice immediately that there is no sign of a bifurcation occurring for any of the Reynolds numbers considered; indeed, it is not obvious from Figure 7.9 whether a bifurcation will ever occur. The values of the eigenvalues are close to zero, but an adaptive strategy using the *a posteriori* error estimator developed in Cliffe *et al.* [11] reveals that the eigenvalues are positive; results for $Re = 1300$, $m = 1$ are shown in Table 7.3.

We now determine the Reynolds number at which a bifurcation occurs by using the adaptive strategy, together with the *a posteriori* error estimator developed in Section

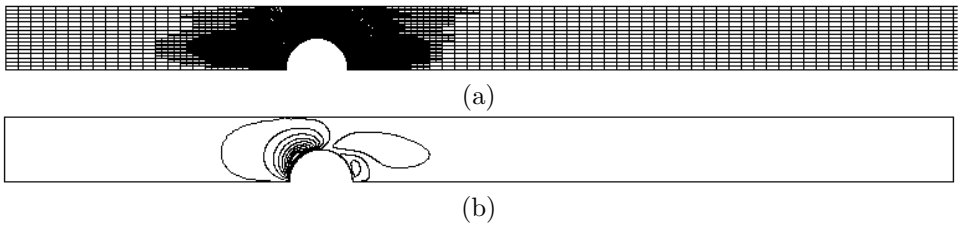

FIG. 7.5. *Example 2: (a) Mesh after 5 refinement steps; (b) Contour plot of* $\mathbf{u}_r^0$.

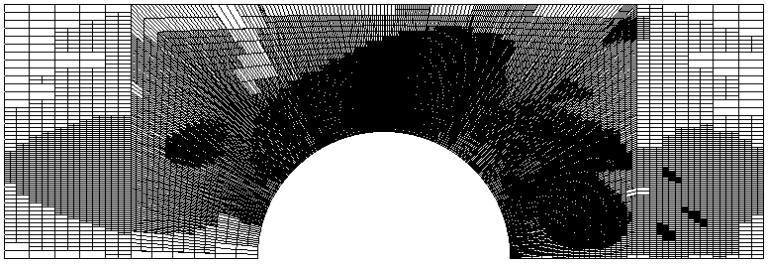

FIG. 7.6. *Example 2: Mesh detail near the blockage.*

4. Here, our initial mesh consists of 15517 elements, graded toward the expansion, with an outlet length of 800 pipe radii. In Table 7.4, we show in tabular form the number of elements, the number of degrees of freedom for both the primal base and primal null solutions, the computed critical Reynolds number $Re_h^0$, and the computed error representation formula. Here, the true error and effectivity indices are not computed, since reliable estimates of the critical Reynolds number are not available. However, our computations indicate that a bifurcation occurs around $Re^0 \approx 5080$. Indeed, on the basis of the computed error representation formula, we would conclude that $Re^0 \approx 5080 \pm 5$. Here, we remark that on the final mesh, we employed 5.9M degrees of freedom for the primal bifurcation problem in order to achieve mesh independent results for $Re_h^0$, at least in the sense that $Re_h^0$ has been computed to three digits of accuracy. Clearly, this level of accuracy would not be achievable by treating the three–dimensional problem directly, without first undertaking the reduction outlined in Section 3. We point out that, on the final mesh we could not compute the solution to the corresponding dual bifurcation problem. By calculating the quantity $d/b_\lambda$ from Lemma 3.6 we determined that the bifurcation detected is supercritical.

While the numerical experiments presented in Table 7.4 indicate the onset of instability at $Re^0 \approx 5080 \pm 5$, we recall that the experimental data published in [25] revealed that the steady symmetric flow becomes asymmetric at Reynolds number $Re^0 = 1139 \pm 10$. Clearly, there is quite a discrepancy between the numerical and experimental results. Further experimental and numerical investigation of this challenging problem still needs to be undertaken in order to fully understand the onset of these asymmetric flows. However, we speculate that at such Reynolds numbers, the problem is highly sensitive to minor perturbations. The analytical reduction undertaken in Section 3 guarantees that the resulting numerical method exactly preserves the $O(2)$ symmetry of the underlying physical problem. In reality, any slight geometrical imperfection in the pipe will violate this key assumption. The investigation of such imperfections can be studied numerically, though this is clearly a very challenging

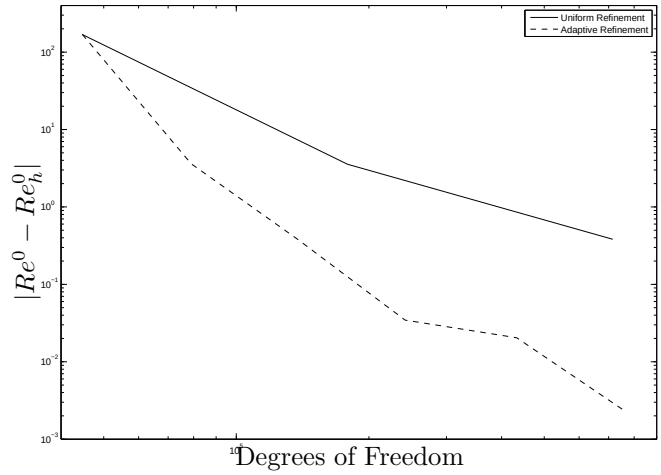


FIG. 7.7. *Example 2: Convergence of the error in the approximation of the critical* $Re^0$.

| Mesh No. | No. Eles | Eig. Dofs | Eigenvalue | Error Estimate |
|---|---|---|---|---|
| 1 | 20000 | 420000 | 0.167241E-02 | 1.741E-06 |
| 2 | 34565 | 725865 | 0.167194E-02 | 1.914E-06 |
| 3 | 65909 | 1384089 | 0.167218E-02 | 9.771E-07 |
| 4 | 111956 | 2351076 | 0.167243E-02 | 5.765E-07 |

TABLE 7.3
*Example 3: Eigenvalue error estimates for* $Re = 1300$ *and* $m = 1$.

problem.

Finally, we now consider the impact the ratio $R_1 : R_2$ has on the location of the bifurcation point. As the critical Reynolds number increases, the length of the required computational domain also increases, hence we are limited to $2 \leq R_2 \leq 3.4$, with $R_1 = 1$. Results with error bars (computed using the *a posteriori* error estimator from Section 4) are shown in Figure 7.10. We notice that as the ratio $R_1 : R_2$ decreases the critical Reynolds number increases, which we may expect because as the ratio becomes smaller we approach a straight pipe. However, more unexpected is the presence of a local minimum at $R_2 \approx 2.6$ with the flow becoming more stable as the ratio is increased further.

**8. Conclusion and outlook.** In this article we have considered the reliable computation of the critical Reynolds number in the numerical approximation of the incompressible Navier-Stokes equations in the case when the underlying system possesses both rotational and reflectional symmetry ($O(2)$ symmetry). Particular attention has been devoted to the *a posteriori* error estimation and adaptive mesh refinement of DG finite element approximations of the associated bifurcation problem, as well as the underlying eigenvalue problem. On the basis of exploiting a duality argument, reliable error estimates of the critical Reynolds number at which a steady pitchfork bifurcation occurs when the underlying physical system possesses $O(2)$ symmetry have been developed. The application of these bounds within an au-

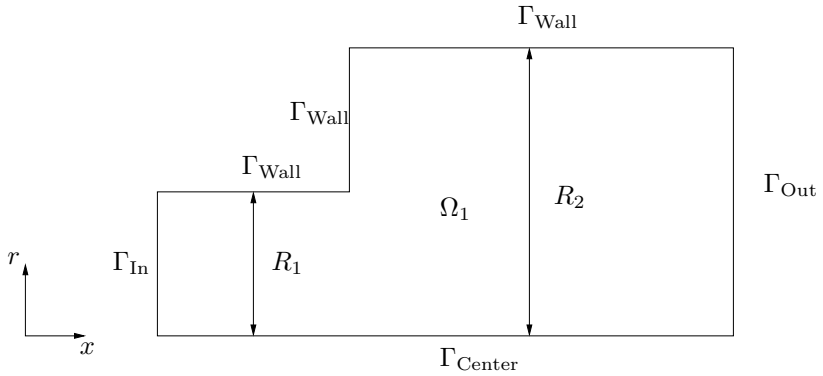


FIG. 7.8. *Example 3: Pipe with a sudden expansion*

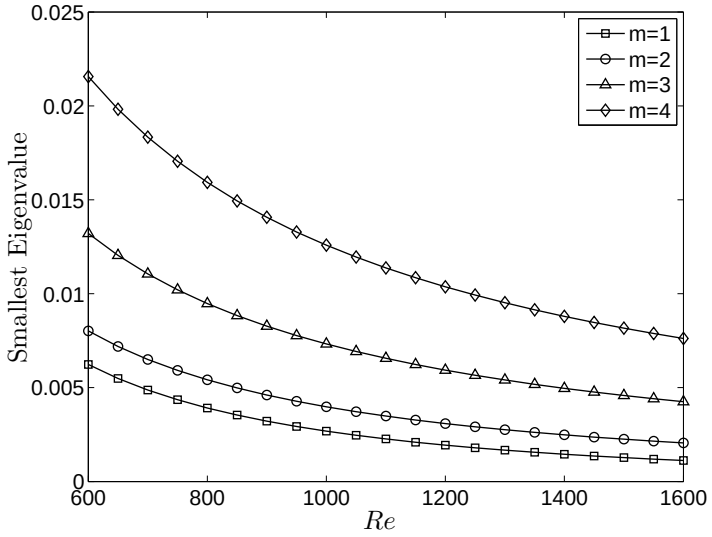


FIG. 7.9. *Example 3: Most dangerous eigenvalue for varying Reynolds number*

tomatic adaptive refinement strategy clearly highlights the flexibility of the proposed *a posteriori* error indicator for accurately locating steady pitchfork bifurcations. The application of these ideas to the challenging problem of flow through a cylindrical pipe with a sudden expansion has been undertaken. In this case, although reliable estimates of the critical Reynolds number have been computed, further work is required to understand the presented computations in light of the experimental work undertaken in the article [25].

**Acknowledgments.** The authors would like to express their gratitude to Prof. T. Mullin (University of Manchester) for his insight and lengthy discussions concerning the flow in the pipe with a sudden expansion. KAC, PH, and EJCH gratefully acknowledge the financial support of the EPSRC under the grant EP/E013724. In addition, all of the authors acknowledge the support of the EPSRC under the grant EP/F01340X.

| Mesh No. | No. Eles | Base Dofs | Null Dofs | $Re_h^0$ | $\lvert\sum \eta_\kappa\rvert$ |
|---|---|---|---|---|---|
| 1 | 15517 | 232755 | 325857 | 4910.17 | 223.49 |
| 2 | 28429 | 426435 | 597009 | 5106.28 | 11.47 |
| 3 | 51499 | 772485 | 1081479 | 5085.25 | 0.77 |
| 4 | 93157 | 1397355 | 1956297 | 5080.59 | 4.14 |
| 5 | 164527 | 2467905 | 3455067 | 5082.41 | - |

TABLE 7.4
*Example 3: Performance of the adaptive algorithm.*

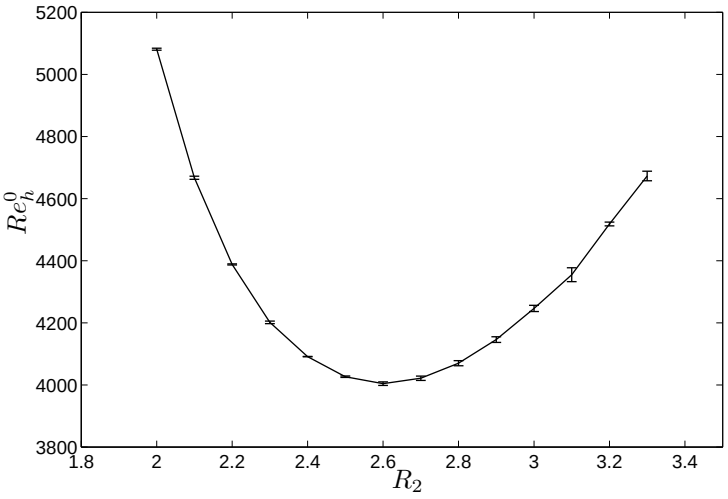


FIG. 7.10. *Example 3: Effect of varying expansion ratio on critical Reynolds number* $Re_h^0$.

## REFERENCES


[1] P. R. Amestoy, I. S. Duff, J. Koster, and J.-Y. L'Excellent. A fully asynchronous multifrontal solver using distributed dynamic scheduling. *SIAM Journal on Matrix Analysis and Applications*, 23(1):15–41, 2001.

[2] P. R. Amestoy, I. S. Duff, and J.-Y. L'Excellent. Multifrontal parallel distributed symmetricand unsymmetric solvers. *Comput. Methods Appl. Mech. Eng.*, 184:501–520, 2000.

[3] P. R. Amestoy, A. Guermouche, J.-Y. L'Excellent, and S. Pralet. Hybrid scheduling for the parallel solution of linear systems. *Parallel Computing*, 32(2):136–156, 2006.

[4] D.N. Arnold, F. Brezzi, B. Cockburn, and L.D. Marini. Unified analysis of discontinuous Galerkin methods for elliptic problems. *SIAM J. Numer. Anal.*, 39:1749–1779, 2001.

[5] P.J. Aston. Analysis and computation of symmetry-breaking bifurcation and scaling laws using group theoretic methods. *SIAM J. Math. Anal.*, 22:139–152, 1991.

[6] R. Becker and R. Rannacher. An optimal control approach to a-posteriori error estimation in finite element methods. In A. Iserles, editor, *Acta Numerica*, pages 1–102. Cambridge University Press, 2001.

[7] H.M. Blackburn, S.J. Sherwin, and D. Barkley. Convective instability and transient growth in steady and pulsatile stenotic flows. *J. Fluid Mech.*, 607:267–277, 2008.

[8] F. Brezzi, J. Rappaz, and P.A. Raviart. Finite dimensional approximation of non-linear problems .3. Simple bifurcation points. *Numer. Math.*, 38(1):1–30, 1981.

[9] K.A. Cliffe, T.J. Garratt, and A. Spence. Eigenvalues of the discretized Navier-Stokes equations with application to the detection of Hopf bifurcations. *Adv. Comp. Math.*, 1:337–356, 1993.

[10] K.A. Cliffe, E. Hall, and P. Houston. Adaptivity and a posteriori error control for bifurcation problems II: Incompressible fluid flow in open systems with $Z_2$ symmetry. *J. Sci. Comput.*

In press.
[11] K.A. Cliffe, E. Hall, and P. Houston. Adaptive discontinuous Galerkin methods for eigenvalue problems arising in incompressible fluid flows. *SIAM J. Sci. Comput.*, 31:4607–4632, 2010.
[12] K.A. Cliffe, E. Hall, P. Houston, E.T. Phipps, and A.G. Salinger. Adaptivity and a posteriori error control for bifurcation problems I: The Bratu problem. *Commun. Comput. Phys.*, 8:845–865, 2010.
[13] K.A. Cliffe, A. Spence, and S.J. Tavener. O(2)-symmetry breaking bifurcation: with application to the flow past a sphere in a pipe. *Internat. J. Numer. Methods Fluids*, 32:175–200, 2000.
[14] B. Cockburn, G. Kanschat, and D. Schötzau. The local discontinuous Galerkin method for the Oseen equations. *Math. Comp.*, 73:569–593, 2004.
[15] B. Cockburn, G. Kanschat, and D. Schötzau. A locally conservative LDG method for the incompressible Navier-Stokes equations. *Math. Comp.*, 74:1067–1095, 2005.
[16] B. Cockburn, G. Kanschat, D. Schötzau, and C. Schwab. Local discontinuous Galerkin methods for the Stokes system. *SIAM J. Numer. Anal.*, 40:319–343, 2002.
[17] K. Eriksson, D. Estep, P. Hansbo, and C. Johnson. Introduction to adaptive methods for differential equations. In A. Iserles, editor, *Acta Numerica*, pages 105–158. Cambridge University Press, 1995.
[18] R.M. Fearn, T. Mullin, and K.A. Cliffe. Nonlinear flow phenomena in a symmetric sudden expansion. *J. Fluid Mech.*, 211:595–608, 1990.
[19] M. Golubitsky and D.G. Schaeffer. *Singularities and Groups in Bifurcation Theory, Vol I.* Springer, New York, 1985.
[20] M. Golubitsky, I. Stewart, and D.G. Schaeffer. *Singularities and Groups in Bifurcation Theory, Vol II.* Springer, New York, 1988.
[21] P. Houston and E. Süli. Adaptive finite element approximation of hyperbolic problems. In T. Barth and H. Deconinck, editors, *Error Estimation and Adaptive Discretization Methods in Computational Fluid Dynamics. Lect. Notes Comput. Sci. Engrg.*, volume 25, pages 269–344. Springer, 2002.
[22] H.B. Keller. *Numerical Solution of Bifurcation and Nonlinear Eigenvalue Problems.* Academic Press, New York, 1977.
[23] M.G. Larson and T.J. Barth. A posteriori error estimation for discontinuous Galerkin approximations of hyperbolic systems. In B. Cockburn, G.E. Karniadakis, and C.-W. Shu, editors, *Discontinuous Galerkin Methods: Theory, Computation and Applications, Lecture Notes in Computational Science and Engineering, Vol. 11.* Springer, 2000.
[24] R.B. Lehoucq, D.C. Sorensen, and C. Yang. *ARPACK USERS GUIDE: Solution of Large Scale Eigenvalue Problems by Implicitly Restarted Arnoldi Methods.* SIAM, Philadelphia, PA, 1998.
[25] T. Mullin, J.R.T. Seddon, M.D. Mantle, and A.J. Sederman. Bifurcation phenomena in the flow through a sudden expansion in a circular pipe. *Phys. Fluids*, 21, 2009.
[26] S.J. Sherwin and H.M. Blackburn. Three–dimensional instabilities and transition of steady and pulsatile axisymmetric stenotics flows. *J. Fluid Mech.*, 533:297–327, 2005.
[27] A. Vanderbauwhede. *Local Bifurcation and Symmetry.* Pitman, 1982.
[28] B. Werner and A. Spence. The computation of symmetry-breaking bifurcation points. *SIAM J. Numer. Anal.*, 21:388–399, 1984.